Test Bench Development and Application to a Parametric Experimental Study on the Dynamic Adsorption Capacity of Noble Gases (Kr, Xe) in the Metal–Organic Framework HKUST-1

Julie Nguyen Sadassivame, Anaïs Massaloux, Jérémy Dhainaut, Riad Sarraf, Philippe Chantereau, Laurent Cantrel, Thierry Loiseau, Christophe Volkringer, Philippe Nérisson

Test Bench Development and Application to a Parametric Experimental Study on the Dynamic Adsorption Capacity of Noble Gases (Kr, Xe) in the Metal-Organic Framework HKUST-1

*Julie Nguyen-Sadassivame[†], Anaïs Massaloux[†], Jérémy Dhainaut[§], Riad Sarraf[‡], Philippe Chantereau[‡], Laurent Cantrel[†], Thierry Loiseau[§], Christophe Volkringer[§] and Philippe Nérisson[†]**

[†]Institut de Radioprotection et de Sûreté Nucléaire/PSN-RES/SEREX/L2EC, BP 3, 13115 Saint-Paul-Lez-Durance Cedex, France

[‡]Nuvia, 85 avenue Archimède, 13290 Aix-en-Provence, France

[§]Univ. Lille, CNRS, Centrale Lille, Univ. Artois, UMR 8181 - UCCS - Unité de Catalyse et Chimie du Solide, F-59000 Lille, France

KEYWORDS: Krypton, xenon, Metal-Organic Frameworks, dynamic adsorption, breakthrough time

ABSTRACT: The objective of this work is to develop a dedicated test bench to study the dynamic noble gases trapping by porous materials, and especially by MOF, in a nuclear context. The well-known copper-containing HKUST-1 material is used to determine the influence of different parameters such as

temperature, concentration, humidity, MOF bed height or diameter, and velocity of the flowrate on noble gases adsorption (Kr, Xe) in breakthrough sorption experiments. Breakthrough time is shown to be directly related to MOF bed height, shaping and gas flow velocity. The adsorption capacities depend on the concentration of noble gases in the gas flow, but also on the flow velocity. Indeed, when the velocity increases from 0.15 to 1 $cm.s^{-1}$, the adsorption capacity of Xe increases from 3.46 to 5.15 $\mu mol.g^{-1}$ at 25 °C and 1 bar, while the breakthrough time decreases from 7.3 to 2.4 min. On the other hand, temperature and the presence of water vapor have a negative effect on noble gas adsorption in HKUST-1.

1. INTRODUCTION

Krypton and xenon are very expensive elements due to their scarcity in the geosphere, but also because of their uses in several industries. They are produced industrially as by-products of the cryogenic distillation of air from nitrogen-oxygen separation process, which is a widespread route though very energy consuming. Since 2022, the war conflict between Russia and Ukraine has also had a negative impact on the commercial availability of Kr and Xe, since these two countries are among the largest world producers of these gases [1].

In terms of application, krypton is a filler gas in incandescent lamps, because it produces high intensity and long-life light. Xenon can also be used as a source of light emission in the form of light flashes (discharge lamps such as camera flash or stroboscopes), as well as for cinema projection systems (IMAX), car headlights and in plasma screens (mixture of xenon and neon ionized by electrodes). Krypton, mixed with argon, is also effective for thermal insulation in double glazing. Some exciplex lasers, used in eye surgery or photolithography in the semiconductor industry, consist of KrF material to give 248 nm ultraviolet radiation. In addition, metastable ^{81}Kr (radioisotope) is used in nuclear medicine to perform lung ventilation scans (medical imaging) or as a contrast agent for medical imaging. The ^{133}Xe radioisotope, on the other hand, makes it possible to measure the blood flow of the heart, lungs or brain by positron

emission tomography (PET). Krypton, like xenon, has a great anesthetic capacity [2]. Indeed, at high concentrations, it limits the oxygen supply. In addition, they generate few side effects (no decrease in blood pressure, faster awakening) because they are evacuated from the body quickly, thanks to their chemical inertness. Among all the noble gases, xenon has the lowest thermal conductivity and first ionization potential. These properties make xenon an excellent candidate for lighting because it minimizes heat loss and puts a lamp into operation more quickly. A final interesting application of xenon is its use as a fuel for space propulsion in ion engines [3]. Indeed, its low ionization energy, its storage in liquid form at high pressure and close to ambient temperature, as well as its ability to return to the gaseous state easily make it possible to power the ion engine. The latter produces its propulsive force by the acceleration of ionized xenon at very high speed (50 km/s) obtained by two highly electrically charged grids (one positively and the other negatively).

The capture and separation of krypton and xenon is also a nuclear safety issue. Indeed, radioactive isotopes such as ^{133}Xe and ^{85}Kr are produced by nuclear fission of uranium and exhibit half-lives of 5.3 days and 10.8 years, respectively. These gases contribute to an accumulation of significant radioactive doses in the environment following nuclear tests, spent nuclear fuel reprocessing, production of medical isotopes or during a hypothetic nuclear severe accident that can occur in nuclear power plant (NPP).

Noble gases chemical inertia and high volatility make them difficult to trap and separate, still their capture using porous materials such as activated carbons or zeolites has been reported in literature [4 5 6 7]. Moreover, for the past ten years, a new class of highly porous hybrid materials called Metal-Organic Frameworks (MOFs) has demonstrated remarkable performance in gas capture, selectivity and storage [8]. In the nuclear plant context, it concerns notably fission

products such as volatile iodine [9] [10] [11] [12] [13] or ruthenium tetroxide [14]. A judicious choice of the metal cluster can also make them resistant to radiations [15] [16]. Two families of studies have been conducted for the capture of noble gases by MOF materials depending on the static or dynamic conditions (*i.e.* gas flow through MOF, less frequently studied) [17].

Numerous studies reported the adsorption of noble gases in porous materials such as MOFs [18] [19] [20] [21], however mostly under so-called static conditions using a gas adsorption analyzer. The experiment consists in inserting a pure gas (Kr or Xe) into the material at a given temperature; then gas-phase pressure variation is measured as a function of the adsorbed gas volume. Literature has highlighted the main parameters for optimizing the adsorption of noble gases in porous materials. The adsorption capacities are reduced when increasing temperature due to the fact that gases become more volatile [22], thus limiting solid-gas interactions. However, they strongly increase with pressure. It is notably highlighted by Mueller *et al.* [23] for noble gases adsorption in MOF-5 at high pressure (15-40 bar). The general trend in the literature shows that the maximum adsorption capacities of noble gases are obtained for materials with high specific surface area (SSA_{BET}), generally greater than 1000 $m^2.g^{-1}$. For example, xenon adsorption record is 7.1 $mmol.g^{-1}$ in PCN-14 (SSA_{BET} = 2138 $m^2.g^{-1}$) and 1.4 $mmol.g^{-1}$ for krypton in NOTT-100 (SSA_{BET} = 1619 $m^2.g^{-1}$) at ambient temperature and pressure [24]. The pore size is an important parameter that can influence the selective adsorption of Xe/Kr [25]. Indeed, when the pore aperture is close to the kinetic diameter of the xenon atom (4.10 Å), the interactions are favored between the gas and the framework or the unsaturated metal sites. Therefore, this makes it possible to create an induced dipole between the electronic cloud of the gas and the MOF. The kinetic diameters of the other gases (N_2, O_2, CO_2, etc.) being smaller, they interact less with the host material. On the other hand, MOFs belonging to this category do not have high adsorption

capacities due to their low specific surface area (generally less than 500 $m^2.g^{-1}$) [26]. The compound SBMOF-1 is a good example with high Xe/Kr selectivity of 16 at 298 K under 1 bar [27]. Indeed, this solid has no unsaturated sites or high porosity (145 $m^2.g^{-1}$), but it presents pore sizes (4.5 Å) very close to the kinetic diameter of the xenon atom. The organic functionalization of the ligand by specific groups also modifies the sorption uptake. For instance, Lee *et al.* [28] investigated the adsorption of krypton and xenon in functionalized UiO-66-X (with X = $-NH_2$, $-(OMe)_2$, $-NH_2(OMe)_2$ and $-F_4$) at 283 K and 1 bar. Xenon adsorption capacity obtained in UiO-66-NH_2 (SSA_{BET} = 1274 $m^2.g^{-1}$) is 2.3 $mmol.g^{-1}$, greater than the original UiO-66 (1.3 $mmol.g^{-1}$) while the specific surface area of the latter is higher (1706 $m^2.g^{-1}$). This ligand functionalization also has an impact on Xe/Kr selectivity ($S_{Xe/Kr}$; see Supporting Information) since it modifies functional groups electron density: $-NH_2(OMe)_2$ ($S_{Xe/Kr}$ = 14.4) > $-NH_2$ ($S_{Xe/Kr}$ = 11.4) > $-(OMe)_2$ ($S_{Xe/Kr}$ = 9.5) > $-F_4$ ($S_{Xe/Kr}$ = 7.4). The adsorption mechanisms involved are the Van der Waals forces because noble gases are uncharged and non-polar while they remain polarizable (Xe more than Kr). This is also shown by Meek *et al.* [29] on the adsorption of Xe and Kr at ambient temperature and pressure on halogenated IRMOF-2 [Zn_4O(2-X-1,4-BDC)$_3$] with X = F, Cl, Br or I. Thus, Xe/Kr selectivity increases with the halogen size in relation to their polarizability: -I ($S_{Xe/Kr}$ = 4.17) > -Br ($S_{Xe/Kr}$ = 3.9) > Cl ($S_{Xe/Kr}$ = 3.7) > F ($S_{Xe/Kr}$ = 3.4). Perry *et al.* [24] studied noble gases adsorption in MOF-74-M series (M = Co, Mg, Ni or Zn), containing open metal sites. They showed that adsorption and interaction energies increase with the polarizability of the gas. MOF-74-Co achieved the best selectivity ($S_{Xe/Kr}$ = 10.4), but no clear trend was defined between interaction energies and the nature of the open metal sites. On the other hand, this type of material obtained overall better performance due to the charge density of the unsaturated sites and its cylindrical and uniform structure (pore size of 11 Å).

Dynamic investigations are much less conducted than static studies [26], but are more adapted to determine a real utilization of adsorbents for industrial applications, like filtration or separation. It involves a gas-mixture flow at different concentrations through a material, under fixed conditions of temperature and pressure (around 298 K and 1 bar for all reported studies). For a porous material, dynamic studies usually lead to lower adsorption capacities than under static conditions. Parameters influencing static adsorption, as previously mentioned, also have an impact on the breakthrough time (*i.e.* time when the target gas is detected downstream the material, at the outlet of the device). The other parameters such as concentration of noble gases, velocity, thickness of MOF bed and presence of water must be considered too.

Liu *et al.* [30] carried out dynamic breakthrough experiments for Kr and Xe sorption, on HKUST-1 and MOF-74-Ni materials. These compounds were selected for their open metal sites, expected to be favorable to noble gases adsorption, and for their different structures and pore sizes. A gas-mixture flow containing 1000 ppmV Xe or 1000 ppmV Kr in air was flowed through the material. The breakthrough times were around 8 min with xenon through both solids, while krypton was detected downstream the MOF almost immediately after injection. Besides, Xe adsorption capacity was slightly higher in MOF-74-Ni (9.3 $\mu mol.g^{-1}$) than in HKUST-1 (8.5 $\mu mol.g^{-1}$), due to the stronger interaction between open metal sites of MOF-74-Ni and Xe. Conversely, Kr adsorption was slightly higher in HKUST-1 (2.0 $\mu mol.g^{-1}$) than in MOF-74-Ni (1.8 $\mu mol.g^{-1}$), owing to its trimodal pore sizes. In addition, this study showed that the gas-mixture concentration influences Xe/Kr selectivity, regardless of the material. Indeed, with 80/20 (V/V) Xe/Kr gas-mixture, the relating Xe/Kr selectivity was lower than with a 20/80 (V/V) Xe/Kr gas mixture Xe/Kr. Selectivity $S_{Xe/Kr}$ under dynamic condition is defined such as:

$$S_{Xe/Kr} = \frac{x_{Xe}/y_{Xe}}{x_{Kr}/y_{Kr}} \quad (1)$$

Where x_i is the adsorbed molar fractions and y_i is the molar fractions in the upstream bulk gas for each species i (i = Kr or Xe).

The material SBMOF-1 [27], mentioned previously, achieved a record breakthrough time of 55 min for Xe and 8 min for Kr, with a 400/40 ppmV Xe/Kr gas-mixture in air. Moreover, this solid presented an exceptional xenon adsorption capacity of 13.2 µmol.g^{-1}. In addition, its low porosity and the absence of unsaturated sites give it great stability, even in the presence of water. Finally, the breakthrough time can be increased by the doping of MOF solids with metallic particles or cations, as conducted by Wang *et al.* [31] on MOF-303 which was silver-doped. Despite a reduced specific surface area of Ag@MOF-303 (716 m².g^{-1}) compared to the initial MOF-303 (1343 m².g^{-1}), the breakthrough time of Xe from a Xe/Kr (20/80 (V/V) gas mixture, was increased by 25 min.cm^{-3}, thanks to the silver doping. Indeed, its pore size also reduces and becomes close to the kinetic diameter of Xe atom (4.7 Å) from 8.7 Å for pristine MOF-303 to 5.2 Å with Ag, which favors Xe retention.

All these dynamic breakthrough experiments were conducted at ambient temperature and pressure, which is not representative of a nuclear accident. In contrast, herein, the objective is to be able to evaluate the effect of severe thermohydraulic conditions over the capture of krypton and xenon by MOF materials.

Indeed, few studies [18 26 32 33] have been carried out under conditions representative of a nuclear accident: flow velocity through material, temperature, humidity, gas mixture, etc… Such data are essential, notably to contribute to improve Filtered Containment Venting Systems (FCVS) [34] implemented on nuclear power plants for mitigation of airborne releases, or equivalent devices in reprocessing plants.

To contribute to this latter point, the present work deals with the development of an experimental test bench allowing the dynamic study of noble gases adsorption (Xe, Kr) by MOFs under nuclear accident conditions listed above. A home-made device named SAFARI (implemented at IRSN-Cadarache-France), initially used for volatile iodine and RuO_4(g) capture [35] [36], has been adapted for the study of noble gases capture, notably with the development of an online analysis method for krypton and xenon gases by gas chromatography coupled with a mass spectrometer. In this work, the reference copper trimesate based material HKUST-1 has been considered and was synthesized.

The HKUST-1 structure consists of paddle-wheel-shaped copper(II) dinuclear units linked by trimesate ligands (noted btc) (Figure 1-A), with the framework chemical formula $[Cu_3(btc)_2]$. The copper atoms are four-fold coordinated through carboxyl oxygens in a square plane, and an additional oxygen atom (water species) occupy the terminal apex of the resulting square pyramidal geometry. The water molecules can be easily desorbed by heating (thermal activation), inducing a color change from light blue (hydrated form) to dark blue/purple (dehydrated form; Figure 1-B). This results in an unsaturated copper site, giving the material its hydrophilic nature. In addition, the porous structure of HKUST-1 delimits three cavity types. Two cavities have a diameter of 13 and 11 Å (cavity volumes represented by yellow and green spheres, respectively) with an opening (cavity access window) of 7 Å. The last type of cavity has a diameter of 5 Å (pink sphere) with an opening of 4 Å, which is close to the kinetic diameters of xenon (4.1 Å) and krypton (3.7 Å) [37].

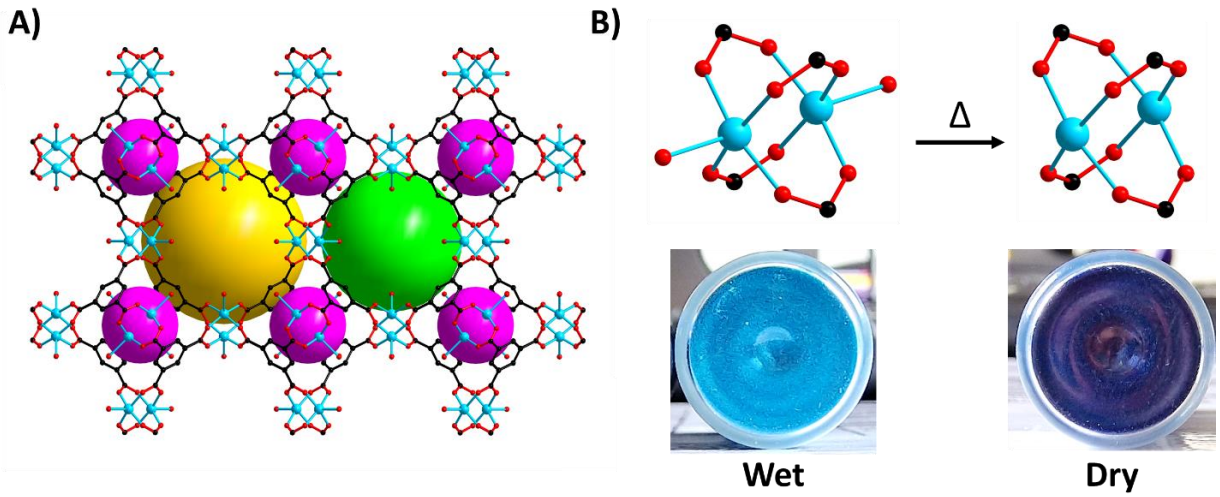

Figure 1. A) Illustration of HKUST-1 structure with different pore sizes (pink: Ø 5 Å, green: Ø 11 Å and yellow: Ø 13 Å). B) Illustration of copper(II) dimer with loss of the terminal water molecule through heating together with photographs of HKUST-1 powdered samples for the hydrated (wet) and dehydrated forms (dry). Copper: blue, oxygen: red and carbon: black. Hydrogen is not represented for clarity.

The copper-based MOF HKUST-1 has been chosen for noble gases trapping study, since it is considered as a reference material, for which synthesis in large-scale quantities is well-known. Besides, the study from Liu *et al.* [30] using HKUST-1 under dynamic conditions at 25 °C and 1 bar can be used as a point of reference for the discussion. They made MOF pellets introduced into a column for a bed aspect ratio about 4-6. Different gas compositions were used: pure Xe or Kr, and Xe/Kr mixtures at 20:80, 50:50 or 80:20 (V/V), diluted to 1000ppmV or 400/40 ppmV Xe/Kr mixture in dry air. The gas flow rates applied were 20, 25 or 50 sccm. The comparison with this study under similar condition will permit to validate SAFARI set-up. In addition, the adsorption capacities of noble gases in dynamic conditions will be compared to those obtained in static conditions. The influence on breakthrough time and adsorption capacities of noble gases (Kr, Xe) of different parameters in dynamic breakthrough experiments (temperature,

concentration in air flow, relative humidity, column diameter, MOF bed height, and gas flow velocity) will be investigated, allowing to determine the main parameters to be considered in dynamic breakthrough experiments of noble gases adsorption by MOF materials

2. MATERIAL AND METHODS

2.1. Synthesis of HKUST-1 material.

The HKUST-1 large-scale synthesis was derived from the protocol proposed by Giovine *et al.* [38]. 238.56 g (1.03 mol) of $Cu(NO_3)_2 \cdot 2.5H_2O$ and 143.14 g (0.68 mol) of trimesic acid were dissolved in 5 L of 50/50 (V/V) water/ethanol liquid mixture, and then placed in a 8 L stainless steel autoclave. The solution was heated at 110 °C during 23 h under mechanical stirring. The obtained suspension was thereafter centrifuged three times with ethanol at 60 °C, to recover blue crystals. These latter were dried at 70 °C during 12 h, prior to be activated at 110 °C during 12 h under vacuum then kept in glove box. The activated material is dark blue/purple, attesting that the material is effectively dried. 220 g of HKUST-1 powder were produced with a specific surface area of 1374 ± 31 $m^2.g^{-1}$ by BET method (characterizations, see Supporting Information).

2.2. Noble gases (Kr, Xe) analysis.

Xe and Kr static adsorption experiments were carried out on a porosity analyzer (Micromeritics ASAP 2020, uncertainly of ± 3%). A Dewar filled with water and connected to an isothermal bath (Pilot One, Huber) was used to keep the temperature at 22, 25 and 50 °C. A Dewar filled with ice and water (v/v = 90/10) was used to maintain the temperature at 0 °C. Pure Xe (99.997% purity, Linde Gas) and Kr (99.9999% purity, Linde Gas) compressed in gas cylinders were used throughout all experiments.

Noble gases dynamic analysis is performed continuously online by gas chromatography coupled to a mass spectrometer (GC-MS). Gas chromatography module (Agilent 7820A, injection split/splitless) is made up of a pre-column (Agilent J&B PoraBond Q with two particle traps) of sizes 3 µm (film thickness) ×0.25 mm (inner diameter) ×25 m (length). The potential

heavy gases (solvents for example) are evacuated through a 6-way valve whereas the light gases (krypton, xenon) reach the second column with molecular sieve (Agilent J&W CP-Molsieve 5 Å) of sizes 30 µm (film thickness) ×25 µm (inner diameter) ×25 m (length). Isotherm analysis is done at 130°C, with a carrier gas flowrate (helium, Air Liquide, 99.99% purity) of 1 $mL.min^{-1}$ in the first column and 5 $mL.min^{-1}$ in the second column. The sampling loop volume (1 mL) is driven by a 6-way valve, with a split ratio of 150:1. The sampling loop is continuously swept by the SAFARI bench outlet gas flow. The 6-way valve is then programmed to inject the volume of the loop into the separation columns using the carrier gas. The uncertainty of the measurement is ± 5%.

The mass spectrometry module (Agilent 5977B GC/MSD) allows ionization of the sample by electron impact (EI) at 230°C and mass analysis by a quadrupole at 150 °C under primary vacuum.

Commercial gas cylinders titrated at 1000 ppmV and 100 ppmV in air (20,9% O_2, 79% N_2, Air Products) of Kr and Xe separately, or 400/40 ppmV Xe/Kr gas mixture, are diluted on a dedicated dilution bench, to obtain standard samples for apparatus calibration and breakthrough experiments.

2.3. Experimental test bench SAFARI

Dynamic breakthrough experiments are carried out on the home-made SAFARI test bench (scheme and pictures in Supporting Information), at IRSN (Institute for Radioprotection and Nuclear Safety, Cadarache, France). This experimental device allows the injection of xenon and/or krypton diluted in air through a bed of adsorbent material. The flow downstream the adsorbent bed is analyzed online by GC-MS (see section 2.2). Before each gas adsorption experiment, the HKUST-1 material is activated at 110 °C for 1 hour in air, under atmospheric pressure. The cylindrical glass column containing a bed of activated HKUST-1 powder on a

sintered filter, is placed in SAFARI test bench. Heating cords and heat insulators are placed around the column, as well as a thermocouple to regulate the temperature. Before and after each xenon and/or krypton breakthrough experiment, the line is swept with dry air at the same velocity of the experiment. Steam can also be added to the gas stream at a desired flowrate (and velocity), to reach the target relative humidity via the steam generator (Bronkhorst, uncertainly of 2% of full scale equal to 10 $g.h^{-1}$). For that, the partial pressure of water is calculated based on the target relative humidity and the water vapor pressure at experiment temperature and pressure. In this way, the water volume ratio is obtained, and its mass flow rate is deduced and applied to the steam generator, heated to the experiment temperature. Gases are injected from the top of the column and a glass bubbler is placed at the outlet to condense the water vapors (for tests involving steam) before injection into the GC-MS. In dynamic experiments, xenon, krypton, or Xe/Kr gas mixture, diluted in air, are injected at a flow controlled (Bronkhorst, uncertainly of 2% of full scale equal to 1 or 0.5 sccm) rate into the glass column through the material. Applied flow rates are calculated using selected flow velocity, column section area, temperature, and pressure of the test. For a typical breakthrough experiment, 1.8 g of anhydrous HKUST-1 is introduced into a 2 cm diameter glass column corresponding to a bed height of 1 cm. The velocity through the MOF is 1 $cm.s^{-1}$ at room temperature (RT) and 1 bar.

Improving the online GC-MS analysis for Kr and Xe was part of this work: the GC-MS outflow gas sampler is programmed to inject a known volume into the separation columns, at periodic intervals. This allows for obtaining a more regular sampling (every 3 min) and a curve with additional points to determine the breakthrough time. This latter corresponds to the time when 5% of the inlet concentration (C_0) is detected downstream the MOF and the saturation is the time when C_0 is recovered.

The sorption capacity could be also calculated with the breakthrough curve. For this, an additional experiment is conducted under the same conditions but with no MOF (called blank). Then, the adsorbed amount (or adsorption capacity named CS) is defined following the Equation 2 by integration of each curve (with and without MOF). This method allows to discriminate the equilibrium time of the death volume of SAFARI to the GC-MS.

$$CS = \frac{Q_v}{V_m W} \int_0^{t_s} \frac{C_{(blank)} - C}{C_{0(blank)} - C_0} dt \quad (2)$$

With CS the adsorbed amount of the gas (mol.g^{-1}), Q_v the injected gas flow rate (m^3.min^{-1}) in the Standard Temperature and Pression (STP), t_s the time of bed saturation (min), C_{blank} and C the Xe or Kr concentrations in the flow for blank test and test with MOF respectively (ppmV), $C_{0(blank)}$ and C_0 the Xe or Kr initial concentration injected for blank test and with MOF respectively (ppmV), V_m the molar volume (m^3.mol^{-1}) in the STP, and W the mass of the activated adsorbent material (g).

3. RESULTS AND DISCUSSION

The porous HKUST-1 compound has been selected for both static and dynamic adsorption of krypton and xenon gases. In a first step, the static adsorption experiment of these two gases has been carried out by using a classical sorption analyzer for powdered porous materials.

In the second step, the dynamic experiments series has been performed on SAFARI bench, which allows to measure different features for noble gases (Xe, Kr) adsorption in HKUST-1, notably the breakthrough time (t_B) and adsorption capacity (CS). Other parameters have been investigated such as:

- temperature (22, 25, 50 and 150 °C) with comparison to static studies at different temperatures (0, 22, 25 and 50 °C);

- concentration of Xe in air flow (50, 400, 500 and 1000 ppmV);
- presence of steam at 50 °C and 150 °C (14%, 30% or 85% Relative Humidity);
- amount of HKUST-1 related to the bed height (1 and 2 cm), column diameter (1 and 2 cm) and compacity;
- velocity of flowrate through the HKUST-1 (0.15, 0.25, 0.90 and 1 $cm.s^{-1}$).

The influence of these points is detailed hereafter. For all experiments, the velocities and noble gases concentrations shown on breakthrough curves, are calculated from the temperature, pressure (downstream) and flowrate measured during the experiment.

3.1. Adsorption of krypton and xenon in HKUST-1 under static conditions.

The adsorption isotherms of the pure krypton and xenon gases are shown in Figure 2, under static conditions. These curves allow to determine Xe and Kr adsorption capacities (CS) and selectivity ($S_{Xe/Kr}$) in HKUST-1 with pressure variation going up to 1.2 bar and at different temperatures (0 °C, 21 °C, 25 °C, 50 °C). The Xe and Kr adsorption capacities are reported in Table 2 with units in $mmol.g^{-1}$ (for comparison with the dynamic studies) whereas they are reported in $cm^3.g^{-1}$ in the Figure 2.

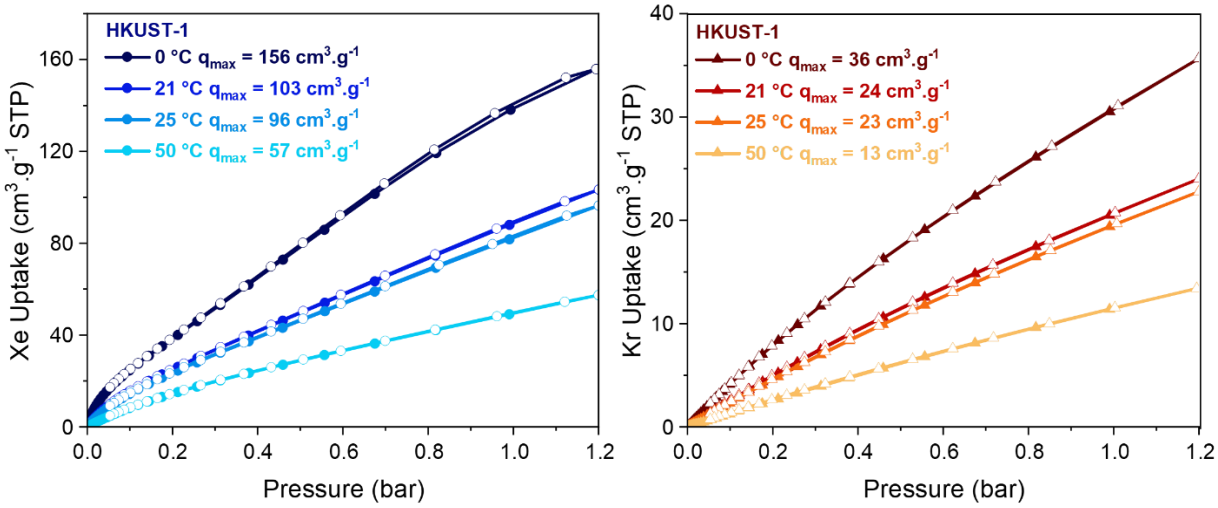

Figure 2. Adsorption/desorption isotherms of xenon (left) and krypton (right) under static conditions in the temperature range 0-50 °C. Adsorption points are full symbol and desorption points are empty symbol. q_{max} is the maximum amount adsorption capacity obtained at 1.2 bar. STP: Standard Temperature and Pressure. Uncertainly ± 3%.

As expected, the volume of noble gases adsorbed decreases when the temperature increases, with significant decreases by factors 3.3 for xenon and 3.1 for krypton in the temperature range 0-50 °C. Thus, the xenon uptake varies from 6.12 mmol.g^{-1} at 0 °C to 1.83 mmol.g^{-1} at 50 °C under 1 bar. The same trend is observed when increasing temperature for krypton, for which the uptake goes from 1.35 mmol.g^{-1} at 0 °C down to 0.43 mmol.g^{-1} at 50 °C under 1 bar. In contrast, the adsorbed volumes of Xe and Kr increase with the pressure without reaching saturation (absence of plateau) at 1.2 bar, the maximum pressure achievable with this instrument. On the other hand, xenon atom is more polarizable than krypton, and due to the cavity sizes in HKUST-1 being relatively close to the kinetic diameter of Xe atom (4.1 Å), xenon is adsorbed four times more than krypton, regardless of the temperature. At ambient temperature (21 °C) and pressure (1 bar), HKUST-1 adsorbs 88.57 cm^3.g^{-1} of Xe (3.62 mmol.g^{-1} or 475.74 mg.g^{-1}) and 21.00 cm^3.g^{-1} of Kr (0.86 mmol.g^{-1} or 71.99 mg.g^{-1}). To compare, the HKUST-1 synthetized by

J.J. Perry IV *et al.* [24] adsorbs 4.60 mmol.g^{-1} of Xe and 1.00 mmol.g^{-1} of Kr at 19 °C under 1 bar. The difference of adsorption capacities with our study comes from the slightly lower temperature of their measurement and their small-scale synthesis leading to a better porosity (1844 m².g^{-1}) than our large-scale synthesis (1374 m².g^{-1}). However, HKUST-1 shows higher Xe adsorption performance than other porous materials. For example, the activated carbon studied by Wang *et al.* [39] adsorbs 3.20 mmol.g^{-1} of Xe at 25 °C and 1 bar, and zeolite ZSM-5 from Yu *et al.* [40] adsorbs 1.69 mmol.g^{-1} of Xe in the same conditions. The adsorption performances of HKUST-1 are explained by the combination of several structural characteristics (adapted pore sizes, unsatured copper sites and high specific surface area).

Experiments under static conditions make it possible to predict selectivity from adsorption isotherms obtained experimentally, despite separately noble gases injection. The Henry's constants reported in Table 1 have been calculated from the equation described in Supporting Information. The selectivity $S_{Xe/Kr}$ (Table 1) follows a variation with the temperature, with values going from 14.6 (at 0 °C) down to 7.8 (at 50 °C). The study by J. J. Perry IV *et al.* [24], shows a selectivity obtained with the same method of 6.9 at 19 °C and 1 bar. This difference with our results certainly comes from the correlation (R^2) of the linear Langmuir equation applied to the experimental adsorption points obtained by J.J. Perry IV (four points between pressure range of 0.01 – 0.09 atm with $R^2 = 0.9624$ for Xe obtained by J.J. Perry IV). Indeed, this correlation depends on the pressure range used and therefore the number of experimental points.

Table 1. Henry's constants ($cm^3.g^{-1}.bar^{-1}$) calculated at different temperatures (0-50 °C) and comparison of the selectivity for the adsorption of Xe over Kr ($S_{Xe/Kr}$) in static and dynamic experiments (400/40 ppmV Xe/Kr in air). Uncertainly ± 3%.

	0 °C	**7 °C**	**19 °C**	**21 °C**	**25 °C**	**50 °C**
$\mathbf{k_{H(Xe)}}$	630.16	-	-	242.14	213.30	91.32
$\mathbf{k_{H(Kr)}}$	43.30	-	-	24.06	23.60	11.76
$\mathbf{S_{Xe/Kr}}$	14.6	-	-	10.1	9.0	7.8
$\mathbf{S_{Xe/Kr}}$ [22]	-	11.8	-	-	-	-
$\mathbf{S_{Xe/Kr}}$ [24]	-	-	6.9	-	-	-

Isosteric heat of adsorption Q_{st}, [22] according to the Equation 3 (Clausius-Clapeyron), is also calculated from static adsorption isotherms of Xe and Kr, using at least three temperatures (here 0, 21, 25 and 50 °C). It is expressed as a function of adsorption volume at different surface coverages (θ) in Figure 3. For a surface coverage (θ) at the limit of zero (Q_{st}^0, Equation 4) calculated from the Henry's constant k_H [41] (from Table 1), the heats of adsorption for xenon and krypton are 28 kJ.mol^{-1} and 19 kJ.mol^{-1}, respectively (determination of Q_{st} and Q_{st}^0, see supporting Information). These values are consistent with the literature (Q_{st}^0 = 27 kJ.mol^{-1} for Xe and Q_{st}^0 = 19 kJ.mol^{-1} for Kr) [22], decrease with the adsorbed gas amount and show the higher affinity of xenon over krypton in HKUST-1. In fact, the interaction force of gases in MOFs are the Van der Waals forces (10-50 kJ.mol^{-1}).

$$Q_{st} = \left| R \left(\frac{\partial(\ln P)}{\partial(1/T)} \right)_{\theta} \right| \quad (3)$$

$$\lim_{n \to 0}(Q_{st}) = \left| R \left(\frac{\partial(\ln k_H)}{\partial(1/T)} \right) \right| \quad (4)$$

With Q_{st} the isosteric heat of adsorption given in absolute value (J.mol^{-1}), R the perfect gas constant (8.314 J.mol^{-1}.K^{-1}), P the pressure (bar), T the temperature (K), θ the surface coverage

($cm^3.g^{-1}$), n the gas quantity adsorbed and k_H the Henry's constant reported in Table 1 ($cm^3.g^{-1}.bar^{-1}$).

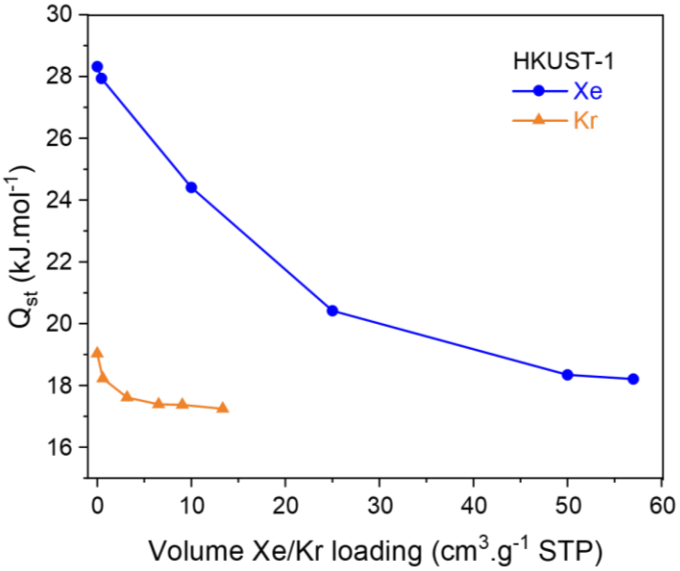

Figure 3. Isosteric heat of adsorption (Q_{st} and Q_{st}^0) for Xe (circle) and Kr (triangle) of HKUST-1 as function of volume of noble gases loading. STP: Standard Temperature and Pressure.

3.2. Influence of temperature.

For the dynamic sorption studies, we first investigated the influence of the experimental temperature. The temperature values of the noble gases adsorption were 22 °C, 50 °C and 150 °C for the injection of a mixture of Xe/Kr at 400/40 ppmV (Figure 4) and for the injection of Xe or Kr at 500 ppmV (Figure in Supporting Information), in dry air at around 1 $cm.s^{-1}$ and 1 bar. The HKUST-1 is disposed as a bed of 1 cm height and 2 cm inner diameter (≈ 1.8 g). The dashed curves correspond to the experiment without material (blank test) and the solid curves are the breakthrough test with HKUST-1.

The evolution of the breakthrough curves shows that the Xe and/or Kr adsorbed amounts decrease upon increasing temperature, whatever the noble gas concentration injected (Xe/Kr mixture at 400/40 ppmV or 500 ppmV of each noble gas). Indeed, the gap between the curves in the presence of HKUST-1 and the blank (without MOF) reduces when the temperature increases,

as expected (see section 3.1). At room temperature (22 °C), xenon breakthrough time is observed at 2.2 min when injected in mixture with Kr (Xe/Kr 400/40 ppmV) and at 3.7 min when injected alone at 500 ppmV. Krypton breakthrough time is almost instantaneous, resulting in a very low adsorption capacity in HKUST-1. In addition, the adsorbed xenon is completely desorbed once the noble gas injection is stopped (desorption phase with air only). Adsorption capacity (Table 2) confirms this trend, xenon amounts being greater than that of krypton. The adsorption capacity of xenon obtained at 22 °C is 5.76 µmol.g^{-1} when injected at 400 ppmV, compared with 8.22 µmol.g^{-1} at 500 ppmV. Thus, the trapping capacities for the injection of 400 ppmV of Xe (in mixture of 40 ppmV of Kr) at 50 °C is 1.00 µmol.g^{-1} and goes down to 0.10 µmol.g^{-1} at 150 °C. For 500 ppmV of Xe injected at 50 °C, 2.08 µmol.g^{-1} are adsorbed, but 0 µmol.g^{-1} at 150 °C. The difference of adsorption capacities between the injection of Xe/Kr 400/40 ppmV gas mixture, and Xe or Kr separately, can be explained by higher concentration injected as discussed below (see section 3.3). It also highlights the most important quantities of noble gases adsorbed in static conditions (order of magnitude mmol.g^{-1}). It is explained that the static experiment used pure gases under pressure, compared to highly diluted flows used in dynamic studies, and attests the influence of the initial concentration injected into the material.

Furthermore, the selectivity obtained at 22 °C is 10.5 for the Xe/Kr mixture at 400/40 ppmV ($S_{Xe/Kr}$ = 2,6 at 50 °C and 2,04 at 150 °C), closely related to the value measured under static conditions ($S_{Xe/Kr}$ = 10.1 at 21 °C; cf. Table 1). This selectivity can be associated to gas atomic diameters compared to pore sizes. Indeed, Xe has a higher polarizability but lower diffusivity than Kr in MOF. This value is higher than data reported by Liu *et al.* [30], where $S_{Xe/Kr}$ = 2.6 obtained with Xe/Kr mixture of pure gases (volume ratio 20:80). This gap can be explained by differences in experimental conditions, especially upstream concentrations (Xe/Kr 20:80 V/V for

Liu et *al.*), gas velocity (not mentioned for Liu *et al*. excepted the flow rate of 50 sccm versus 1 $cm.s^{-1}$ with flow rate of 183 sccm) through the HKUST-1 and its shaping (pellet for Liu versus powder form here). Liu *et al.* also mention a selectivity of 8.1 in HKUST-1 predicted with GCMC simulation by Ryan *et al.* [42]. The latter ratio is attributed to a theoretical equilibrium selectivity calculated by the simulation, whereas experimental selectivity is a combination of equilibrium and kinetic selectivity.

Table 2. Comparison of Xe and Kr adsorption capacities (CS) in HKUST-1 in static and dynamic conditions under 1 bar and temperature (T) range of 0 - 150 °C (1 cm bed height with 2 cm inner diameter at 1 $cm.s^{-1}$ for our dynamic work).

	CS_{xenon}		$CS_{krypton}$		
T (°C)	Static ($cm^3.g^{-1}$/$mmol.g^{-1}$)	Dynamic ($\mu mol.g^{-1}$)	Static ($cm^3.g^{-1}$ /$mmol.g^{-1}$)	Dynamic ($\mu mol.g^{-1}$)	Ref.
0	138.91/6.12	-	30.64/1.35	-	This work
19	-/4.60	-	-/1.00	-	[24]
21	89.28/3.64	-	20.60/0.84	-	This work
22	-	0.50[a]	-	-	This work
22	-	5.76[e]	-	0.13[e]	This work
22	-	8.22[b]	-	0.00[b]	This work
25	82.62/3.33	5.15[b]	19.43/0.78	-	This work
25	-	9.73[c]	-	-	This work
25	-	8.50[d]	-	2.00[d]	[30]
50	49.14/1.83	1.00[e]	11.55/0.43	0.00[e]	This work
50	-	2.08[b]		0.00[b]	This work
150	-	0.10[e]	-	0.01[e]	This work
150		0.00[b]		0.00[b]	This work

[a] 50 ppmv Xe in air
[b] 500 ppmV of Xe or Kr in air
[c] 1000 ppmV Xe in air
[d] 1000 ppmV of Xe or Kr in air at a flow rate of 20 sccm
[e] 400/40 ppmV Xe/Kr in air

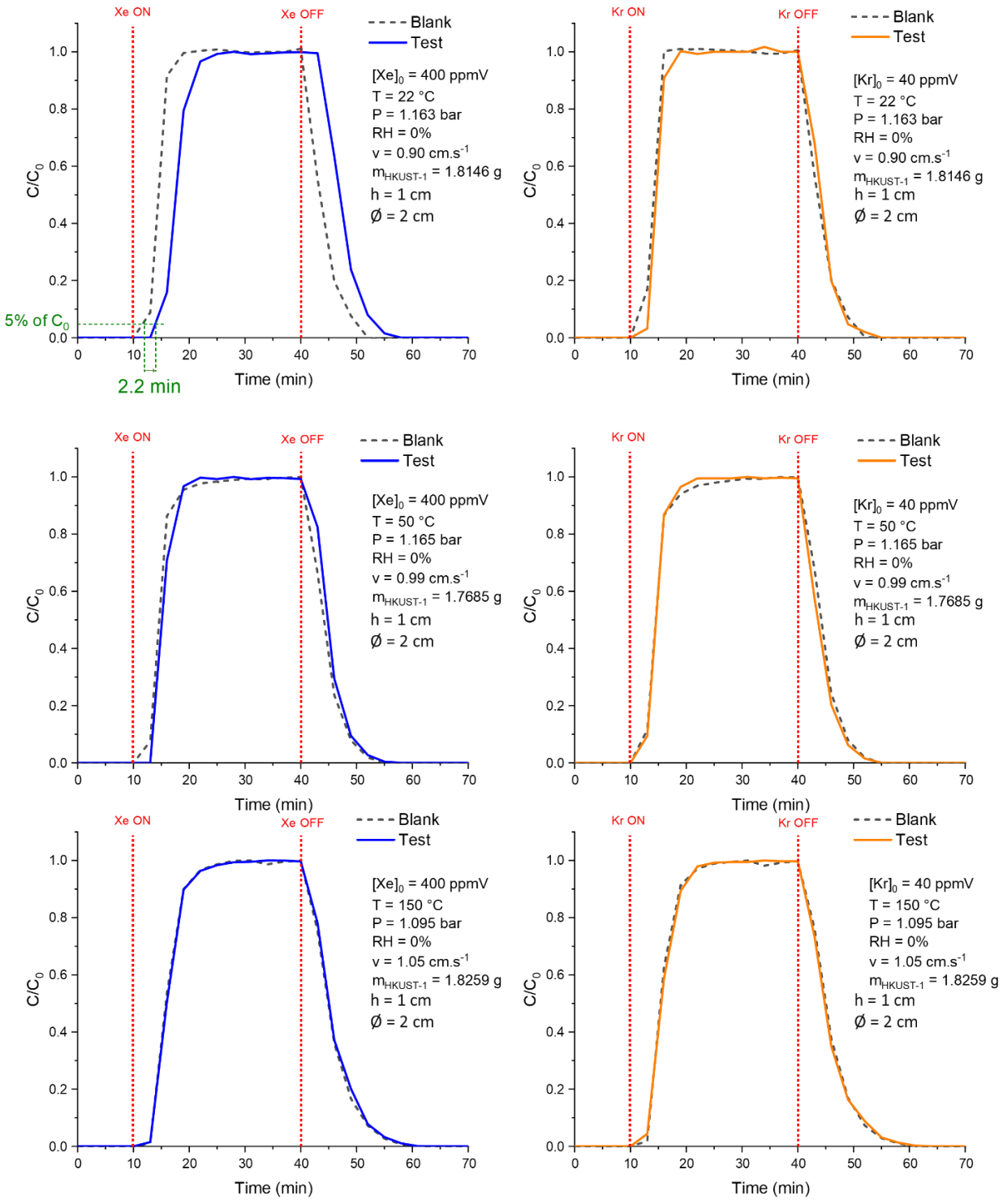

Figure 4. Xe (left) and Kr (right) breakthrough curves in HKUST-1 material on SAFARI test bench from a mixture of Xe/Kr (400/40 ppmV in air), as function of temperature (T): 22 °C (top), 50 °C (middle) and 150 °C (bottom). The dashed curves are the test without MOF (blank)

and solid curves are with (test). Pressure (P) ≈ 1 bar. Velocity (v) ≈ 1 cm.s^{-1}. Bed height (h) = 1 cm. Column inner diameter (Ø) = 2 cm. HKUST-1 mass (m) ≈ 1.8 g. Uncertainly ± 5%.

3.3. Influence of concentration.

The comparison between dynamic and static studies at different temperatures shows, as expected, a larger adsorption uptake of xenon compared to that observed for krypton, as well as a difference in adsorption capacity when it is injected pure or diluted within the material. Table 3 compares the influence of the injected xenon concentration (50, 400, 500 and 1000 ppmV in air), at 1 cm.s^{-1} and room temperature, on its adsorption in HKUST-1 (1 cm bed height with 2 cm inner diameter). The breakthrough curve for 50 ppmV Xe is presented in section 3.5. and for 500-1000 ppmV at 25 °C in Supporting Information.

The results show identical breakthrough times, whatever the initial concentration, on the order of 2.5 min, except for C_0 = 500 ppmV Xe. This can be explained by the limited number of measurement points during breakthrough (10 points over 30 min due to injection times every 3 min, ideal time, in the GC-MS analysis method). On the other hand, the initial xenon concentration influences the quantity adsorbed by HKUST-1. Indeed, since the adsorption capacity of pure gas under static conditions is of the order of mmol.g^{-1} at equal pressure (see section 3.1), the material is still far enough away from its maximum storage capacity for dilute concentrations, due to its large specific surface area (1374 m².g^{-1}).

Table 3. Comparison of breakthrough time (t_B) and adsorption capacities (CS) in HKUST-1 at different inlet concentrations of Xe (50-1000 ppmV) in air flow at room temperature (T).

C_0 Xe (ppmV)	T (°C)	P (bar)	v ($cm.s^{-1}$)	CS_{Xe} ($\mu mol.g^{-1}$)	t_B (min)
50	22	1.16	0.91	0.50	2.5
400*	22	1.17	0.99	5.76	2.2
500	22	1.17	0.98	8.22	3.7
500	25	1.02	1.00	5.15	2.4
1000	25	1.16	1.00	9.73	2.5

* Injected with 40 ppmV of Kr

Pressure (P) ≈ 1 bar. Velocity (v) ≈ 1 $cm.s^{-1}$. Bed height (h) = 1 cm. Column inner diameter (Ø) = 2 cm. HKUST-1 mass ≈ 1.8 g.

3.4. Influence of humidity.

In the event of a severe accident in a nuclear reactor and the use of the containment depressurization line, the flow evacuated through the FCVS may contain a significant amount of water steam (from 30%w to 80%w). The SAFARI bench makes it possible to approach these conditions and observe the influence of humidity on the adsorption of noble gases by MOFs.

Table 4 summarizes the adsorption capacities and breakthrough times obtained for filtration of a 500 ppmV of xenon flow (velocity 1 $cm.s^{-1}$) by HKUST-1 (1 cm bed height with 2 cm inner diameter). Three different relative humidity (RH) levels are injected: 30% and 85% at 50 °C, and 14% at 150 °C (maximum achievable value at this temperature due to the mass flow controller with Qm_{max} = 10 $g_{steam}.h^{-1}$). Figure 5 shows the breakthrough curves obtained, together with photographs showing the colour evolution of HKUST-1 during the tests (starting from a dehydrated form, *i.e* dark blue/purple).

Table 4: Comparison of breakthrough time (t_B) and adsorption capacities (CS) of xenon (500 ppmV in air) on HKUST-1 under dry air flow and in the presence of 30%, 85% RH (at 50 °C) and 14% RH (at 150 °C).

RH (%)	H_2O (%w)	Total m_{H2O} (g)	Qm_{H20} ($g.h^{-1}$)	T (°C)	P (bar)	v ($cm.s^{-1}$)	CS_{Xe} ($\mu mol.g^{-1}$)	t_B (min)
-	-	-	-	50	1.17	0.98	2.08	1.7
30	1.9	0,14	0.28	50	1.18	1.01	1.29	0.3
85	5.7	0,43	0.85	50	1.18	1.08	2.09	0.3
14	47.8	4,81	9.61	150	1.12	2.48	0.00	0.0

m_{H2O}: total mass of water injected, $\%_w$: volume percentage of water corresponding and Q_{mH2O}: mass flow rate of water applied to the steam generator. Pressure (P) ≈ 1 bar. Velocity (v) ≈ 1 $cm.s^{-1}$. Bed height (h) = 1 cm. Column inner diameter (Ø) = 2 cm. HKUST-1 mass ≈ 1.8 g.

The addition of water vapor and its condensation prior to GC-MS analysis modifies volume flow rate calculations. Therefore, the xenon adsorption tests (Figure 5) show real injected concentrations, lower than the initial C_0 concentration considered in dry air (500 ppmV). In addition, the steam generator flow rate shows a slight variation (particularly at low mass flow rates), which can be observed in the shape of some breakthrough curves (bumps).

Despite these instabilities, the tests using water steam demonstrate the reduction in xenon adsorption uptakes compared with those under the same conditions without steam. The amount adsorbed by HKUST-1 is 1.29 $\mu mol.g^{-1}$ with 30% RH (or 1.9%$_w$ of water) at 50 °C, compared with 2.08 $\mu mol.g^{-1}$ in same conditions without steam. This can be explained by the competition on adsorption site of HKUST-1 between Xe and H_2O molecules because of its high polarizability. Similarly, breakthrough times of Xe were 1.7 min without steam and 0.3 min with 30% RH (or 1.9%$_w$ of water) at 50 °C. The test with 85% RH (or 5.7%$_w$ of water) at 50 °C is however inconclusive due to the instability of the steam generator, visible on its breakthrough

curve with a inconsistent point at t ≈ 15 min, causing an overestimation of the quantity adsorbed, also far from that desorbed ($CS_{ads/des}$ = 2.09/0.87 µmol.g^{-1}).

In addition, pictures of the powdered HKUST-1 samples were taken during the test before, during and after xenon injection under humidity. HKUST-1, initially anhydrous (dark blue/purple), is hydrophilic due to its open copper metal sites, where water adsorbs and gives the MOF its light blue color. Thus, Figure 5-A and 7-B show that HKUST-1 is dry (dark blue) before injection of the Xe/H_2O(g) mixture, then turns light blue at 10 and 20 min during the adsorption phase. However, during the desorption phase, notably when xenon is no longer detected by GC-MS (complete desorption), HKUST-1 is still light blue, indicating the presence of water at least connected to copper atoms. This means that water molecules are competing with xenon for adsorption sites. As water is a polar molecule, adsorption is thus favoured. On the other hand, at 150 °C and 14% RH (or 47.8 $\%_w$ of water), the HKUST-1 remained dark blue (*i.e.* dry) and MOF "agglomerates" were formed (as observed in Figure 5-C). In addition, xenon trapping at 150 °C is however not observed, as seen previously.

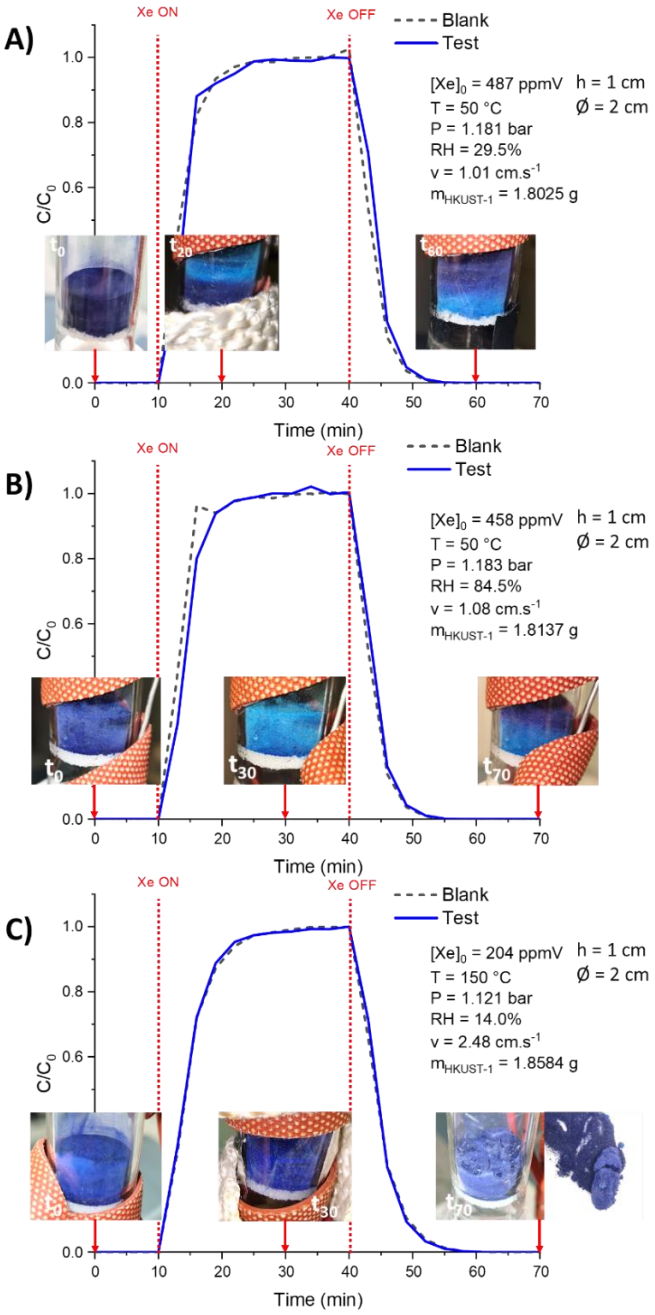

Figure 5. Xenon breakthrough curves in HKUST-1 material on SAFARI test bench for inlet concentration of 500 ppmV in air flow with different percentages of relative humidity (RH). A) 30% RH at 50 °C. B) 85% RH at 50 °C. C) 14% RH at 150 °C. Pictures of HKUST-1 at different time of the experiment (0, 20-30 and 60-70 min). The dashed curves are the test without MOF (blank) and solid curves are with (test). Pressure (P) ≈ 1 bar. Velocity (v) ≈ 1-2.5 $cm.s^{-1}$. Bed

height (h) = 1 cm. Column inner diameter (Ø) = 2 cm. HKUST-1 mass ≈ 1.8 g. Uncertainly ± 5%.

Figure 6 shows a broadening of the Bragg peaks on the X-ray diffraction diagrams of HKUST-1, after exposure to steam water, whatever the relative humidity level of the injected flux. This crystallinity loss is confirmed by a decrease of BET specific surface area values from the nitrogen adsorption/desorption isotherms at 77 K (Figure 6). Indeed, the specific surface area of HKUST-1 after synthesis is 1374 $m^2.g^{-1}$. The specific surface after contact with water steam still remains higher than 1000 $m^2.g^{-1}$, with 1045 $m^2.g^{-1}$ after exposure to 30% RH (or 1.9%w of water), 1181 $m^2.g^{-1}$ after 85% RH (or 5.7%w of water) and 1193 $m^2.g^{-1}$ after 14% RH (or 47.8%w of water). These results are in agreement with the observations made by Giovine *et al.* [38] where a partial collapse of HKUST-1 structure was shown in the presence of water, but this is attenuated for temperatures above 100 °C. In this case, water adsorption is inhibited, thus limiting the hydrolysis process. In addition, the review by Nicholas *et al.* [43] demonstrated that MOF stability with water depends on exposure time (thermodynamic stability in aqueous solution) and the conditions under which the solid is exposed (kinetic stability under humidity).

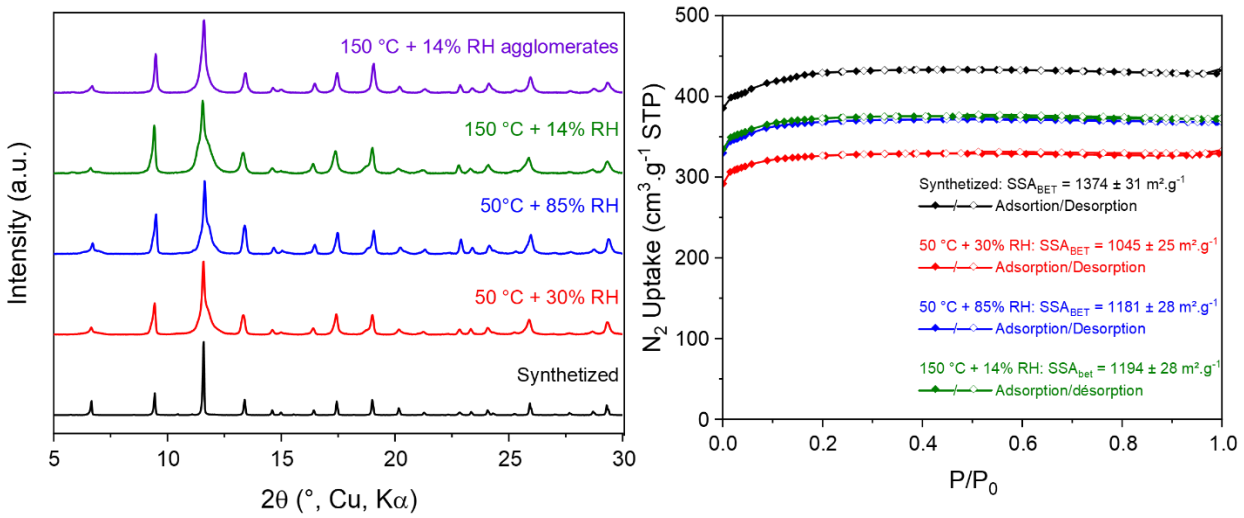

Figure 6. Powder XRD patterns (left) and N_2 adsorption-desorption isotherms at 77 K (right) of HKUST-1 as synthetized and after 30-85% RH (at 50 °C) and 14% RH (at 150 °C) exposure.

To support these hypotheses, SEM images were taken and are shown in Supporting Information. After exposure to 30% RH at 50 °C, the HKUST-1 surface appears to undergo a crystalline phase change as described by Giovine *et al.* [38]. After exposure to 85% RH, at the same temperature, no significant change was observed. Nevertheless, the crystal surface appears rougher. On the other hand, when tested at high temperature (150 °C) and 14% RH, the surface condition remains unchanged, but the crystals were cracked.

3.5. Influence of amount of HKUST-1.

In this section, the dimensioning of the MOF bed is studied. We therefore modified the HKUST-1 bed, by changing either the height (h = 1 or 2 cm), the inner diameter (Ø = 1 or 2 cm) or the compactness of its powder (manual compaction pressed at 12 $kg.cm^{-2}$). For the latter parameter, the aim is to determine whether a material in pellet form could provide better xenon or krypton trapping. These tests were carried out for xenon injection (50 or 500 ppmV) in dry air at room temperature (22-25 °C). The adsorption capacities and breakthrough times are given in

Table 5. Breakthrough curves for changes in bed height are shown in Figure 7 and for changes in bed inner diameter in Supporting Information.

Table 5. Comparison of breakthrough time (t_B) and adsorption capacities (CS) of Xe (50 ppmV or 500 ppmV) in HKUST-1 at different MOF bed heights (1 or 2 cm), bed diameters (1 or 2 cm) and compactnesses, at ambient temperature (T).

Mass of HKUST-1 (g)	h (cm)	Ø (cm)	C_0 Xe (ppmV)	T (°C)	P (bar)	v ($cm.s^{-1}$)	CS_{Xe} ($\mu mol.g^{-1}$)	t_B (min)
1.81	1	2	50	22	1.16	0.91	0.50	2.5
3.59	2	2	50	22	1.17	0.91	0.63	5.4
0.79	1	1	500	22	1.02	1.00	4.20	2.6
1.85	1	2	500	25	1.02	1.00	5.15	2.4
0.49 (powder)	1	1	500	25	1.02	1.00	3.13	1.1
0.67 (compacted)	1	1	500	25	1.02	1.00	2.44	2.3

Pressure (P) ≈ 1 bar. Velocity (v) ≈ 1 $cm.s^{-1}$.

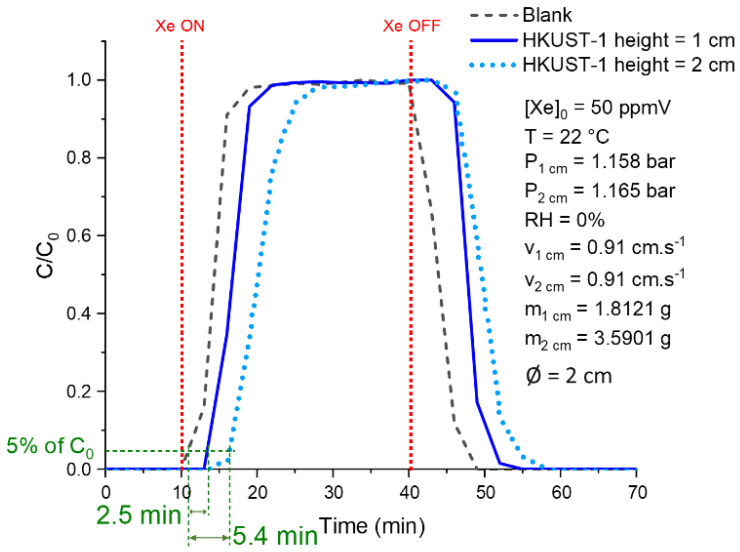

Figure 7. Xenon breakthrough curves in HKUST-1 material on SAFARI test bench for inlet concentration of 50 ppmV in air, as function of MOF height: 1 cm (line curve) and 2 cm (dot curve). The dashed curves are the test without MOF (blank). Pressure (P) ≈ 1 bar. Velocity (v) ≈ 1 $cm.s^{-1}$. Column inner diameter (Ø) = 2 cm. HKUST-1 mass (m) ≈ 1.8 or 3.6 g. Uncertainly ± 5%.

According to the results, when the bed height is doubled, the adsorption capacity is slightly increased, from 0.50 $\mu mol.g^{-1}$ for a height of 1 cm, to 0.63 $\mu mol.g^{-1}$ for 2 cm. On the other hand, breakthrough time is doubled from 2.5 min to 5.4 min. So, for the same velocity through the MOF bed, the residence time of xenon in the MOF increases with the height of the bed. When the column diameter is doubled, the residence time in HKUST-1 bed remains identical (same velocity), so as expected, breakthrough times remain equal. Besides, adsorption capacity is increased (4.20 $\mu mol.g^{-1}$ for Ø = 1 cm and 5.15 $\mu mol.g^{-1}$ for Ø = 2 cm), due to the greater quantity of MOF inserted in the column. As a result, breakthrough time is closely linked to MOF

bed height rather than diameter, with no significant impact on the quantity adsorbed in either case.

The HKUST-1 compactness has also been studied by pressing the powdered sample directly into the 1 cm diameter column, using a 0.75 cm diameter glass rod. This is placed on a balance to determine the weight applied, equal to 12 kg for 5 min, to obtain a height of 1 cm. The pressure applied is 2.69 MPa, calculated according to Equation 5, for a mass of 0.67 g of HKUST-1, compared with 0.49 g with no force applied (h = 1 cm). These two tests, with and without compactness, are then compared.

$$P = \frac{F}{S} = \frac{m.g}{\frac{\pi.d^2}{4}} \quad (5)$$

With P the pressure (MPa), F the force (N), S the surface (mm), m the mass (kg), g the gravity (9,81 $m.s^{-2}$) et d the diameter (mm).

The results show a longer breakthrough time with this shaping (2.3 min versus 1.1 min without). This is due to a pressure upstream the bed of 1.326 bar when the material is pressed, much higher than without shaping (1.034 bar). This higher upstream pressure reflects the higher aeraulic resistance of the bed (difficulty for the flow to pass through HKUST-1). Indeed, the material is denser, and the xenon breakthrough time is longer. On the other hand, trapping capacity was not increased with the shaped material. The xenon trapping capacity obtained is 2.44 $\mu mol.g^{-1}$, compared with 3.13 $\mu mol.g^{-1}$ when HKUST-1 was inserted in powder form. This difference can be explained by a slight loss of crystallinity following pelletizing (increase in peak width at half-height, with values varying from 0.1878° not compacted – to 0.2374° (2θ) - compacted), as observed in the XRD diagrams (Figure 8), where broadening is visible on the peaks at 2.6°, 9.5°, 11.7° and 13.4°.

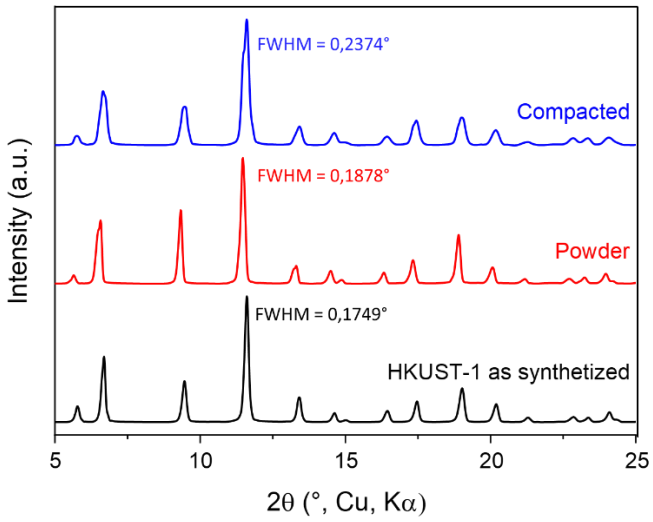

Figure 8. Powder XRD patterns of HKUST-1 as-synthetized (bottom), powder (middle) and compacted at 2.69 MPa (top). FWHM: full width at half maximum (radiation: copper wavelength).

This shaping study can be compared with the dynamic study reported by Liu *et al.* [30]. Indeed, their study concerns the dynamic filtration of xenon at 1000 ppmV in air at 25 °C, where HKUST-1 is pelletized (pressed at 12 MPa) but the height was not specified. The xenon adsorption capacity obtained by Liu *et al*. is 8.50 µmol.g^{-1} (Qv_{tot} = 20 sccm) with a breakthrough time of 8 min. This test is comparable to the one carried out and described in section 3.3, where conditions are similar (1000 ppmV Xe in air at 22 °C). The adsorbed quantity obtained (CS_{ads} = 9.73 µmol.g^{-1}) is relatively close to that of the Liu *et al.*, in contrast to the 2.5 min breakthrough time. The difference may therefore be due to the HKUST-1 pelletizing, since it has been shown in this section that breakthrough time is directly correlated with bed height and shaping. On the other hand, this difference in breakthrough time may also be linked to the pressures and velocities in the HKUST-1. Indeed, their breakthrough experiment involves a helium sweep, before and after the injection of 1000 ppmV of xenon diluted in air. During bench development, the influence of the sweep gas was demonstrated to cause changes in pressure and hence flow

velocity. Furthermore, the velocity applied in the experiment reported by Liu *et al.* is not clearly mentioned, and the absence of bed dimensions makes it impossible to calculate it with the flow rate indicated and go ahead for deeper interpretations.

3.6. Influence of velocity.

The influence of the flow rate through HKUST-1 has been studied in order to determine the variation of xenon (500 ppmV) adsorption uptake in air at room temperature (25 °C). Four velocities were tested, ranging from 0.15 $cm.s^{-1}$ to 1 $cm.s^{-1}$, on an uncompacted HKUST-1 bed (height: 1 cm; diameter: 2 cm). The results are gathered in Table 6 and for 0.15, 0.25 and 1 $cm.s^{-1}$, the breakthrough curves are presented in Supporting Information.

Table 6. Comparison of breakthrough time (t_B) and adsorption capacities (CS) of xenon (500 ppmV in air) at room temperature (T) in HKUST-1 at different flow rate velocities (0.15, 0.25, 0.91 and 1 $cm.s^{-1}$) calculated at experiment temperature (T) and pressure (P).

Velocity ($cm.s^{-1}$)	T (°C)	P (bar)	CS_{Xe} ($\mu mol.g^{-1}$)	t_B (min)
0.15	25	1.00	3.46	7.3
0.25	25	1.03	3.81	4.7
0.91	22	1.17	8.22	3.7
1.00	25	1.21	5.15	2.4

Bed height (h) = 1 cm. Column inner diameter (Ø) = 2 cm. HKUST-1 mass ≈ 1.8 g.

As the flow velocity increases, the residence time within the porous material decreases, resulting in a shorter xenon breakthrough time, as discussed in section 3.5 (influence of bed height). Thus, at a velocity of 0.15 $cm.s^{-1}$, xenon breakthrough time is 7.3 min, compared with 2.4 min at the highest velocity tested (1 $cm.s^{-1}$). The breakthrough time obtained at 0.15 $cm.s^{-1}$ is

close to that obtained by the team of Liu *et al.* [30] (8 min), despite the difference in shaping (here in non-compacted powder form).

Surprisingly, the results show an increase of the adsorbed xenon amount as a function of flow velocity in HKUST-1. At low velocities (0.15 $cm.s^{-1}$), the solid adsorbs 3.46 $\mu mol.g^{-1}$ and up to 5.15 $\mu mol.g^{-1}$ at 1 $cm.s^{-1}$. For an intermediate velocity of 0.91 $cm.s^{-1}$, the adsorption capacity of xenon rises to 8.22 $\mu mol.g^{-1}$, but this experiment was carried at a lower temperature (22 °C). It was previously shown that the temperature decreasing induces higher xenon uptakes (see section 3.2). This trend observed in the Table 6 is attributed to the higher pressure (upstream of the bed, measured on SAFARI test bench) as velocity increases. This allows xenon atoms to diffuse into the pores of HKUST-1. Thus, this diffusivity is, by nature, velocity-dependent, as observed here for xenon.

This phenomenon is demonstrated by Parkes *et al.* [44] in their molecular dynamics simulation of influence of loading of atoms and force field on noble gases diffusion in MOFs. Their aim was to observe the diffusion trend of noble gases (Ar, Xe and Kr) in HKUST-1 and ZIF-8, in order to improve the modeling of this phenomenon. Gas atom diffusion occurs mainly via jumping between the material cages, particularly in HKUST-1, due to its larger cavities and access windows compared to ZIF-8 (4 × 12 Å). Their conclusion is that Xe and Kr diffusion in HKUST-1 depends on two factors: the steric effect of the framework, which decreases diffusion as the noble gas content increases, and the effect of small cavities, which, conversely, increases diffusion.

The flow velocity is then a significant parameter to be determined for each material studied, in order to consider the diffusion of the noble gas within it. Moreover, this diffusion phenomenon is already considered in gas chromatography in order to determine the optimum elution velocity to

obtain the best separation efficiency depending on the column [45]. This parameter is not always clearly mentioned in the literature as well as the choice of the applied flow rates. However, it is an essential parameter in the study of noble gases adsorption to compare different porous materials such as MOFs, since various gas adsorption capacities are observed when varying the velocity.

4. CONCLUSIONS

This work aims to develop a specific test bench to be able to determine the krypton and xenon trapping capacity under dynamic gas flow into porous materials, with different experimental conditions, such as temperature, concentration, gas mixture, relative, humidity, geometrical dimensions and quantity of the sample, and velocity. **A home-made SAFARI setup has been designed with the use of GC-MS on-line method for noble gases analysis in order to proceed to dynamic breakthrough experiments.** A reference Metal-Organic Framework (MOF) porous material named HKUST-1 has been selected, synthetized, and structurally characterized, to evaluate its noble gases adsorption capacities under dynamic conditions. Literature review made it possible to highlight the main parameters influencing the adsorption capacities of krypton or xenon into MOFs, as well as their trapping selectivity.

In a first step, **the static study demonstrated an adsorption capacity of xenon about four times greater than krypton, whatever the temperature due to the higher polarizability of Xe and the pore sizes of HKUST-1**, close to the kinetic diameter of the Xe atom. This is confirmed by adsorption enthalpies, calculated from adsorption isotherms, equal to 28 $kJ.mol^{-1}$ for Xe and 19 $kJ.mol^{-1}$ for Kr. Due to the temperature-dependent volatility of the gas, the amount adsorbed is favored at low temperatures. Thus, Xe uptake varies from 6.12 $mmol.g^{-1}$ at 0 °C and

decrease to 1.83 mmol.g^{-1} at 50 °C (under 1 bar). The Henry selectivity Xe/Kr was calculated to 10.1 at 21 °C.

Following this, **a dynamic study on SAFARI device highlighted the different parameters to be considered in the development of this type of bench, dedicated to the adsorption capacities and the breakthrough times of noble gases through porous materials. Thus, the breakthrough time of the gas depends on the bed height, its shaping and the flow velocity**. Indeed, when the bed height is increased by a factor 2, the residence time of the gas into the MOF increases and the breakthrough time is twice as long (from 2.5 to 5.4 min). Likewise, when the velocity is reduced (1 to 0.15 cm.s^{-1}), it allows a longer breakthrough time of the gas (2.5 to 7.3 min). Shaping, with the powder pressed at 2.69 MPa, reduces the crystallinity of the MOF and therefore the quantity adsorbed, but increases its density and therefore the gas breakthrough time. In fact, it is more difficult for the flow to cross the bed, where a higher upstream pressure is measured. Pressures are important parameters to indicate for comparisons between studies, especially when the sweep gas is different from the noble gas matrix, as observed during the bench development. This is the case in the literature, where helium is used before and after the dilute noble gas is injected into the air. This generates pressure variations, hence modifies flow velocity due to the density of the gas. The adsorption capacity of noble gas (Xe, Kr) depends on the initial concentration injected into the MOF and on the flow velocity. Due to the high specific surface area of HKUST-1 (1374 m².g^{-1}), the solid has a high gas storage capacity (order of magnitude: mmol.g^{-1}), demonstrated in static conditions with the injection of pure Xe or Kr. In addition, the selectivity Xe/Kr obtained is 10.5 for 400/40 ppmV Xe/Kr mixture in air at room temperature, consistent with the static study. However, injection of dilute noble gases (order of magnitude ppmV) does not enable saturation of the material, with adsorption capacities in the

order of magnitude of µmol.g^{-1}. On the other hand, higher flow velocities (0.15 to 1 cm.s^{-1}), *i.e.* lower residence times, allow better gas diffusion within HKUST-1's porous cavities, thus favoring noble gas adsorption (3.46 to 5.15 µmol.g^{-1} at room temperature under 1 bar). It is essential to determine the optimum velocity for each material studied to optimize the quantity of noble gas trapped. Increasing the height or diameter of the bed can also lead to a slight increase in the quantity trapped, due to the greater presence of material. Finally, temperature and the presence of steam water have a negative impact on the breakthrough time and adsorption capacity of noble gases into HKUST-1. Indeed, temperature increases gas volatility and thus reduces trapping, which is consistent with static study. As for water molecules, due to competition on HKUST-1 adsorption sites and the hydrophilic nature of the solid, they limit the adsorption of noble gases. In addition, hydrolysis of the framework leads to structural alteration and loss of MOF.

In conclusion, the parameters studied in this work are important elements to consider when developing this type of bench and comparing material performance. **Breakthrough time is closely linked to bed dimensions, while adsorption capacity depends on the nature of the MOF and test conditions. A compromise must therefore be made in order to achieve high noble gases capture and breakthrough times to reach more representative conditions of the nuclear severe accident context.** The Xe and Kr adsorption study performed with HKUST-1 provides very encouraging results, allowing a test bench validation. In outlook, additional tests with regenerated materials could be considered, to be compared to the results obtained with new materials. Besides, the co-adsorption of CO_2 [46] (as well as other poisoning molecules like NOx) in HKUST-1 cannot be ruled out and will be investigated in near future investigations.

ASSOCIATED CONTENT

Characterization of HKUST-1 material, scheme and pictures of the experimental test bench, breakthrough curves, calculations of selectivity Xe/Kr and isosteric heat of adsorption are available in Supporting Information.

AUTHOR INFORMATION

Corresponding Author

* E-mail: philippe.nerisson@irsn.fr

ORCID

Julie Nguyen-Sadassivame: 0000-0002-0801-922X

Jérémy Dhainaut: 0000-0002-1035-0114

Laurent Cantrel: 0000-0002-9854-967X

Philippe Nerisson: 0000-0002-5078-745X

Thierry Loiseau: 0000-0001-8175-3407

Christophe Volkringer: 0000-0003-2769-9360

Author Contributions

The manuscript was written through contributions of all authors. All authors have given approval to the final version of the manuscript.

Notes

The authors declare no competing financial interest.

ACKNOWLEDGMENTS

This work was performed with the financial support of NUVIA Company. The authors thank the UPCAT facility at UCCS laboratory for their contribution to the large-scale synthesis of HKUST-1. The CNRS, the Chevreul Institute (FR 2638), the Ministère de l′Enseignement Supérieur et de la Recherche, the Région Hauts-de-France, and the FEDER are acknowledged for supporting this work.

REFERENCES

(1) Lebedev, P.; Pryanichnikov, V. Present and Future Production of Xenon and Krypton in the Former USSR Region and Some Physical Properties of These Gases. *Nuclear Instruments and Methods in Physics Research Section A: Accelerators, Spectrometers, Detectors and Associated Equipment* **1993**, *327* (1), 222–226.

(2) Goto, T.; Nakata, Y.; Ishiguro, Y.; Niimi, Y.; Suwa, K.; Morita, S. Minimum Alveolar Concentration-Awake of Xenon Alone and in Combination with Isoflurane or Sevoflurane. *Anesthesiology* **2000**, *93* (5), 1188–1193. https://doi.org/10.1097/00000542-200011000-00009.

(3) Patterson, M.; Benson, S. NEXT Ion Propulsion System Development Status and Performance. *43rd AIAA/ASME/SAE/ASEE Joint Propulsion Conference & Exhibit* **2007**, 5199. https://doi.org/10.2514/6.2007-5199.

(4) Bazan, R. E.; Bastos-Neto, M.; Moeller, A.; Dreisbach, F.; Staudt, R. Adsorption Equilibria of O2, Ar, Kr and Xe on Activated Carbon and Zeolites: Single Component and Mixture Data. *Adsorption* **2011**, *17* (2), 371–383. https://doi.org/10.1007/s10450-011-9337-3.

(5) Munakata, K.; Kanjo, S.; Yamatsuki, S.; Koga, A.; Ianovski, D. Adsorption of Noble Gases on Silver-Mordenite. *Journal of Nuclear Science and Technology* **2003**, *40* (9), 695–697.

(6) Ianovski, D.; Munakata, K.; Kanjo, S.; Yokoyama, Y.; Koga, A.; Yamatsuki, S.; Tanaka, K.; Fukumatsu, T.; Nishikawa, M.; Igarashi, Y. Adsorption of Noble Gases on H-Mordenite.

Journal of Nuclear Science and Technology **2002**, *39* (11), 1213–1218. https://doi.org/10.1080/18811248.2002.9715313.

(7) Underhill, D. W. The Adsorption of Argon, Krypton and Xenon on Activated Charcoal. *Health Phys.* **1996**, *71* (2), 160–166. https://doi.org/10.1097/00004032-199608000-00006.

(8) Ma, S.; Zhou, H.-C. Gas Storage in Porous Metal–Organic Frameworks for Clean Energy Applications. *Chemical Communications* **2010**, *46* (1), 44–53.

(9) Leloire, M.; Dhainaut, J.; Devaux, P.; Leroy, O.; Desjonqueres, H.; Poirier, S.; Nerisson, P.; Cantrel, L.; Royer, S.; Loiseau, T.; Volkringer, C. Stability and Radioactive Gaseous Iodine-131 Retention Capacity of Binderless UiO-66-NH2 Granules under Severe Nuclear Accidental Conditions. *Journal of Hazardous Materials* **2021**, *416*, 125890. https://doi.org/10.1016/j.jhazmat.2021.125890.

(10) Chebbi, M.; Azambre, B.; Monsanglant-Louvet, C.; Marcillaud, B.; Roynette, A.; Cantrel, L. Effects of Water Vapour and Temperature on the Retention of Radiotoxic CH3I by Silver Faujasite Zeolites. *Journal of Hazardous Materials* **2021**, *409*, 124947. https://doi.org/10.1016/j.jhazmat.2020.124947.

(11) Sava, D. F.; Rodriguez, M. A.; Chapman, K. W.; Chupas, P. J.; Greathouse, J. A.; Crozier, P. S.; Nenoff, T. M. Capture of Volatile Iodine, a Gaseous Fission Product, by Zeolitic Imidazolate Framework-8. *J. Am. Chem. Soc.* **2011**, *133* (32), 12398–12401. https://doi.org/10.1021/ja204757x.

(12) Xie, W.; Cui, D.; Zhang, S.-R.; Xu, Y.-H.; Jiang, D.-L. Iodine Capture in Porous Organic Polymers and Metal–Organic Frameworks Materials. *Mater. Horiz.* **2019**, *6* (8), 1571–1595. https://doi.org/10.1039/C8MH01656A.

(13) Jin, K.; Lee, B.; Park, J. Metal-Organic Frameworks as a Versatile Platform for Radionuclide Management. *Coordination Chemistry Reviews* **2021**, *427*, 213473. https://doi.org/10.1016/j.ccr.2020.213473.

(14) Chibani, S.; Badawi, M.; Loiseau, T.; Volkringer, C.; Cantrel, L.; Paul, J.-F. A DFT Study of RuO4 Interactions with Porous Materials: Metal–Organic Frameworks (MOFs) and Zeolites. *Phys. Chem. Chem. Phys.* **2018**, *20* (24), 16770–16776. https://doi.org/10.1039/C8CP01950A.

(15) Volkringer, C.; Falaise, C.; Devaux, P.; Giovine, R.; Stevenson, V.; Pourpoint, F.; Lafon, O.; Osmond, M.; Jeanjacques, C.; Marcillaud, B.; Sabroux, J. C.; Loiseau, T. Stability of Metal–Organic Frameworks under Gamma Irradiation. *Chem. Commun.* **2016**, *52* (84), 12502–12505. https://doi.org/10.1039/C6CC06878B.

(16) Hastings, A. M.; Fairley, M.; Wasson, M. C.; Campisi, D.; Sarkar, A.; Emory, Z. C.; Brunson, K.; Fast, D. B.; Islamoglu, T.; Nyman, M.; Burns, P. C.; Gagliardi, L.; Farha, O. K.; Hixon, A. E.; LaVerne, J. A. Role of Metal Selection in the Radiation Stability of Isostructural M-UiO-66 Metal–Organic Frameworks. *Chem. Mater.* **2022**, *34* (18), 8403–8417. https://doi.org/10.1021/acs.chemmater.2c02170.

(17) Gabrielli, F.; Herranz, L. E.; Paci, S. Proceedings of the 10th European Review Meeting on Severe Accidents Research (ERMSAR2022): Severe Accident Research Eleven Years after the Fukushima Accident. *European Review Meeting on Severe Accidents Research (ERMSAR2022) Conference* **2022**.

(18) Jin, K.; Lee, B.; Park, J. Metal-Organic Frameworks as a Versatile Platform for Radionuclide Management. *Coordination Chemistry Reviews* **2020**, *427*, 213473. https://doi.org/10.1016/j.ccr.2020.213473.

(19) Abramova, A.; Couzon, N.; Leloire, M.; Nerisson, P.; Cantrel, L.; Royer, S.; Loiseau, T.; Volkringer, C.; Dhainaut, J. Extrusion-Spheronization of UiO-66 and UiO-66_NH2 into Robust-Shaped Solids and Their Use for Gaseous Molecular Iodine, Xenon, and Krypton Adsorption. *ACS Applied Materials & Interfaces* **2022**, *14* (8), 10669–10680.

(20) Li, G.; Ji, G.; Wang, X.; Liu, W.; Zhang, D.; Chen, L.; He, L.; Liang, S.; Li, X.; Ma, F. Efficient and Selective Capture of Xenon over Krypton by a Window-Cage Metal–Organic Framework with Parallel Aromatic Rings. *Separation and Purification Technology* **2022**, *295*, 121281.

(21) Wang, X.; Ma, F.; Liu, S.; Chen, L.; Xiong, S.; Dai, X.; Tai, B.; He, L.; Yuan, M.; Mi, P.; Gong, S.; Li, G.; Tao, Y.; Wan, J.; Chen, L.; Sun, X.; Tang, Q.; He, L.; Yang, Z.; Chai, Z.; Wang, S. Thermodynamics-Kinetics-Balanced Metal–Organic Framework for In-Depth Radon Removal under Ambient Conditions. *J. Am. Chem. Soc.* **2022**, *144* (30), 13634–13642. https://doi.org/10.1021/jacs.2c04025.

(22) Soleimani Dorcheh, A.; Denysenko, D.; Volkmer, D.; Donner, W.; Hirscher, M. Noble Gases and Microporous Frameworks; from Interaction to Application. *Microporous and Mesoporous Materials* **2012**, *162*, 64–68. https://doi.org/10.1016/j.micromeso.2012.06.004.

(23) Mueller, U.; Schubert, M.; Teich, F.; Puetter, H.; Schierle-Arndt, K.; Pastre, J. Metal–Organic Frameworks—Prospective Industrial Applications. *Journal of Materials Chemistry* **2006**, *16* (7), 626–636.

(24) Perry IV, J. J.; Teich-McGoldrick, S. L.; Meek, S. T.; Greathouse, J. A.; Haranczyk, M.; Allendorf, M. D. Noble Gas Adsorption in Metal–Organic Frameworks Containing Open Metal Sites. *The Journal of Physical Chemistry C* **2014**, *118* (22), 11685–11698.

(25) Wang, X.; Ma, F.; Xiong, S.; Bai, Z.; Zhang, Y.; Li, G.; Chen, J.; Yuan, M.; Wang, Y.; Dai, X. Efficient Xe/Kr Separation Based on a Lanthanide–Organic Framework with One-Dimensional Local Positively Charged Rhomboid Channels. *ACS Applied Materials & Interfaces* **2022**, *14* (19), 22233–22241.

(26) Banerjee, D.; Simon, C. M.; Elsaidi, S. K.; Haranczyk, M.; Thallapally, P. K. Xenon Gas Separation and Storage Using Metal-Organic Frameworks. *Chem* **2018**, *4* (3), 466–494. https://doi.org/10.1016/j.chempr.2017.12.025.

(27) Banerjee, D.; Simon, C. M.; Plonka, A. M.; Motkuri, R. K.; Liu, J.; Chen, X.; Smit, B.; Parise, J. B.; Haranczyk, M.; Thallapally, P. K. Metal–Organic Framework with Optimally Selective Xenon Adsorption and Separation. *Nature Communications* **2016**, *7* (1), 11831. https://doi.org/10.1038/ncomms11831.

(28) Lee, S.-J.; Kim, S.; Kim, E.-J.; Kim, M.; Bae, Y.-S. Adsorptive Separation of Xenon/Krypton Mixtures Using Ligand Controls in a Zirconium-Based Metal-Organic Framework. *Chemical Engineering Journal* **2018**, *335*, 345–351. https://doi.org/10.1016/j.cej.2017.10.155.

(29) Meek, S. T.; Teich-McGoldrick, S. L.; Perry, J. J.; Greathouse, J. A.; Allendorf, M. D. Effects of Polarizability on the Adsorption of Noble Gases at Low Pressures in Monohalogenated Isoreticular Metal–Organic Frameworks. *The Journal of Physical Chemistry C* **2012**, *116* (37), 19765–19772.

(30) Liu, J.; Thallapally, P. K.; Strachan, D. Metal–Organic Frameworks for Removal of Xe and Kr from Nuclear Fuel Reprocessing Plants. *Langmuir* **2012**, *28* (31), 11584–11589. https://doi.org/10.1021/la301870n.

(31) Wang, H.; Shi, Z.; Yang, J.; Sun, T.; Rungtaweevoranit, B.; Lyu, H.; Zhang, Y.; Yaghi, O. M. Docking of CuI and AgI in Metal–Organic Frameworks for Adsorption and Separation of Xenon. *Angewandte Chemie* **2021**, *133* (7), 3459–3463.

(32) Liu, J.; Fernandez, C. A.; Martin, P. F.; Thallapally, P. K.; Strachan, D. M. A Two-Column Method for the Separation of Kr and Xe from Process Off-Gases. *Ind. Eng. Chem. Res.* **2014**, *53* (32), 12893–12899. https://doi.org/10.1021/ie502156h.

(33) Nandanwar, S. U.; Coldsnow, K.; Utgikar, V.; Sabharwall, P.; Eric Aston, D. Capture of Harmful Radioactive Contaminants from Off-Gas Stream Using Porous Solid Sorbents for Clean Environment – A Review. *Chemical Engineering Journal* **2016**, *306*, 369–381. https://doi.org/10.1016/j.cej.2016.07.073.

(34) Jacquemain, D.; Guentay, S.; Basu, S.; Sonnenkalb, M.; Lebel, L.; Ball, J.; Allelein, H.; Liebana, M.; Eckardt, B.; Losch, N. *OECD/NEA/CSNI Status Report on Filtered Containment Venting*; 45089842; Organisation for Economic Co-Operation and Development, **2014**.

(35) Nerisson, P.; Hu, H.; Paul, J. F.; Cantrel, L.; Vesin, C. Filtration Tests of Gaseous Ruthenium Tetroxide by Sand Bed and Metallic Filters. *J Radioanal Nucl Chem* **2019**, *321* (2), 591–598. https://doi.org/10.1007/s10967-019-06612-8.

(36) Leloire, M.; Nerisson, P.; Pourpoint, F.; Huvé, M.; Paul, J.-F.; Cantrel, L.; Loiseau, T.; Volkringer, C. Capture and Immobilization of Gaseous Ruthenium Tetroxide RuO 4 in the UiO-66-NH 2 Metal–Organic Framework. *Dalton Transactions* **2022**, *51* (42), 16170–16180.

(37) Sikora, B. J.; Wilmer, C. E.; Greenfield, M. L.; Snurr, R. Q. Thermodynamic Analysis of Xe/Kr Selectivity in over 137000 Hypothetical Metal–Organic Frameworks. *Chemical Science* **2012**, *3* (7), 2217–2223.

(38) Giovine, R.; Pourpoint, F.; Duval, S.; Lafon, O.; Amoureux, J.-P.; Loiseau, T.; Volkringer, C. The Surprising Stability of Cu3(Btc)2 Metal–Organic Framework under Steam Flow at High Temperature. *Crystal Growth & Design* **2018**, *18* (11), 6681–6693. https://doi.org/10.1021/acs.cgd.8b00931.

(39) Wang, Q.; Xiong, S.; Xiang, Z.; Peng, S.; Wang, X.; Cao, D. Dynamic Separation of Xe and Kr by Metal-Organic Framework and Covalent-Organic Materials: A Comparison with Activated Charcoal. *Sci. China Chem.* **2016**, *59* (5), 643–650. https://doi.org/10.1007/s11426-016-5582-3.

(40) Yu, Y.; Li, X.; Min, X.; Shang, M.; Tao, P.; Sun, T. Influences of Channel Morphology and Brønsted Acidity on ETS-10, ZSM-5, and SSZ-13 for Xenon and Krypton Separation. *Journal of Environmental Chemical Engineering* **2022**, *10* (1). https://doi.org/10.1016/j.jece.2021.106982.

(41) Yang, R. T. *Adsorbents: Fundamentals and Applications*; John Wiley & Sons, 2003.

(42) Ryan, P.; Farha, O. K.; Broadbelt, L. J.; Snurr, R. Q. Computational Screening of Metal-Organic Frameworks for Xenon/Krypton Separation. *AIChE Journal* **2011**, *57* (7), 1759–1766. https://doi.org/10.1002/aic.12397.

(43) Burtch, N. C.; Jasuja, H.; Walton, K. S. Water Stability and Adsorption in Metal–Organic Frameworks. *Chem. Rev.* **2014**, *114* (20), 10575–10612. https://doi.org/10.1021/cr5002589.

(44) Parkes, M. V.; Demir, H.; Teich-McGoldrick, S. L.; Sholl, D. S.; Greathouse, J. A.; Allendorf, M. D. Molecular Dynamics Simulation of Framework Flexibility Effects on Noble Gas Diffusion in HKUST-1 and ZIF-8. *Microporous and Mesoporous Materials* **2014**, *194*, 190–199. https://doi.org/10.1016/j.micromeso.2014.03.027.

(45) Marriott, P. J. GAS CHROMATOGRAPHY | Principles. In *Encyclopedia of Analytical Science (Second Edition)*; Worsfold, P., Townshend, A., Poole, C., Eds.; Elsevier: Oxford, **2005**; pp 7–18. https://doi.org/10.1016/B0-12-369397-7/00218-1.

(46) Hamon, L.; Jolimaître, E.; Pirngruber, G. D. CO2 and CH4 Separation by Adsorption Using Cu-BTC Metal− Organic Framework. *Industrial & Engineering Chemistry Research* **2010**, *49* (16), 7497–7503.

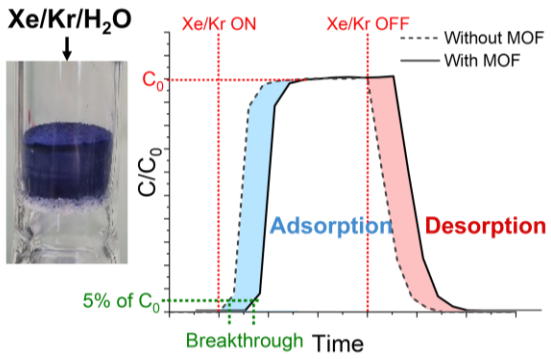

Supporting Information

*Julie Nguyen-Sadassivame[†], Anaïs Massaloux[†], Jérémy Dhainaut[§], Riad Sarraf[‡], Philippe Chantereau[‡], Laurent Cantrel[†], Thierry Loiseau[§], Christophe Volkringer[§] and Philippe Nérisson[†]**

[†]Institut de Radioprotection et de Sûreté Nucléaire/PSN-RES/SEREX/L2EC, BP 3, 13115 Saint-Paul-Lez-Durance Cedex

[‡]Nuvia, 85 avenue Archimède, 13290 Aix-en-Provence, France

[§]Univ. Lille, CNRS, Centrale Lille, Univ. Artois, UMR 8181 - UCCS - Unité de Catalyse et Chimie du Solide, F-59000 Lille, France

KEYWORDS: Krypton, xenon, Metal-Organic Frameworks, adsorption, dynamic study, breakthrough time

1. Characterization of HKUST-1 material

Powder X-ray diffraction diagram has been collected at ambient temperature using a diffractometer Bruker D8 Advance A25. N_2 adsorption-desorption isotherm at 77 K until 1 bar has been measured with a Micromeritics ASAP 2020 porosimeter. BET specific surface is calculated on the range $0.015 \leq P/P_0 \leq 0.30$. Before measurement, the material is heated under a primary vacuum (5 Pa) at 110 °C during 12 h. This heating device is also used for static adsorption experiments of noble gases. Figure S9 presents the PXRD diagram, N_2 adsorption-desorption isotherm, TGA curve and SEM picture of as-synthetized HKUST-1.

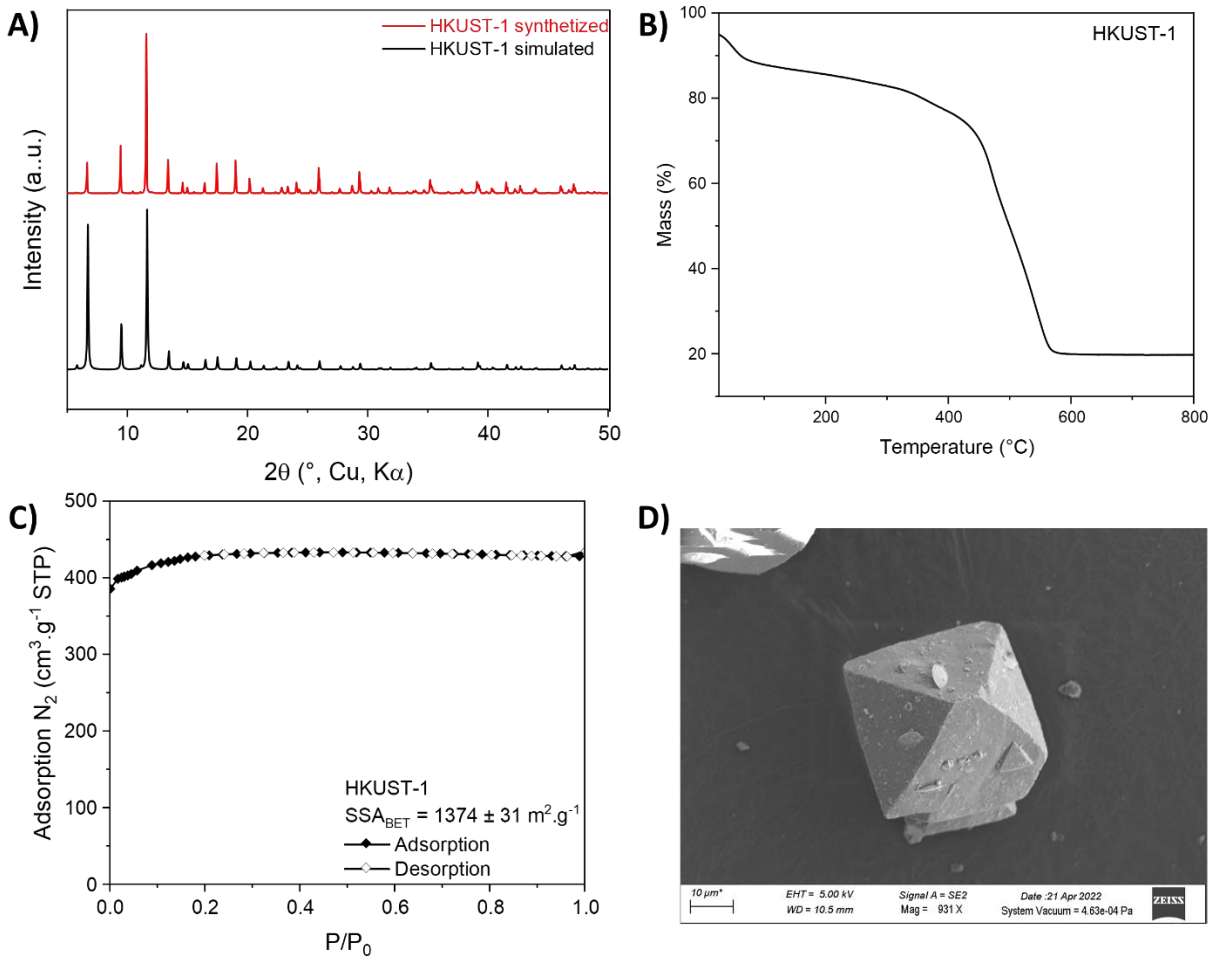

Figure S9. A) PXRD patterns of activated HKUST-1 (top) and reference (bottom). Radiation: copper wavelength. B) TGA curve. C) N_2 adsorption-desorption isotherm at 77 K, where the BET surface area was calculated to be 1374 ± 31 $m^2.g^{-1}$. D) SEM picture of octahedral crystal of HKUST-1.

2. Experimental test bench SAFARI

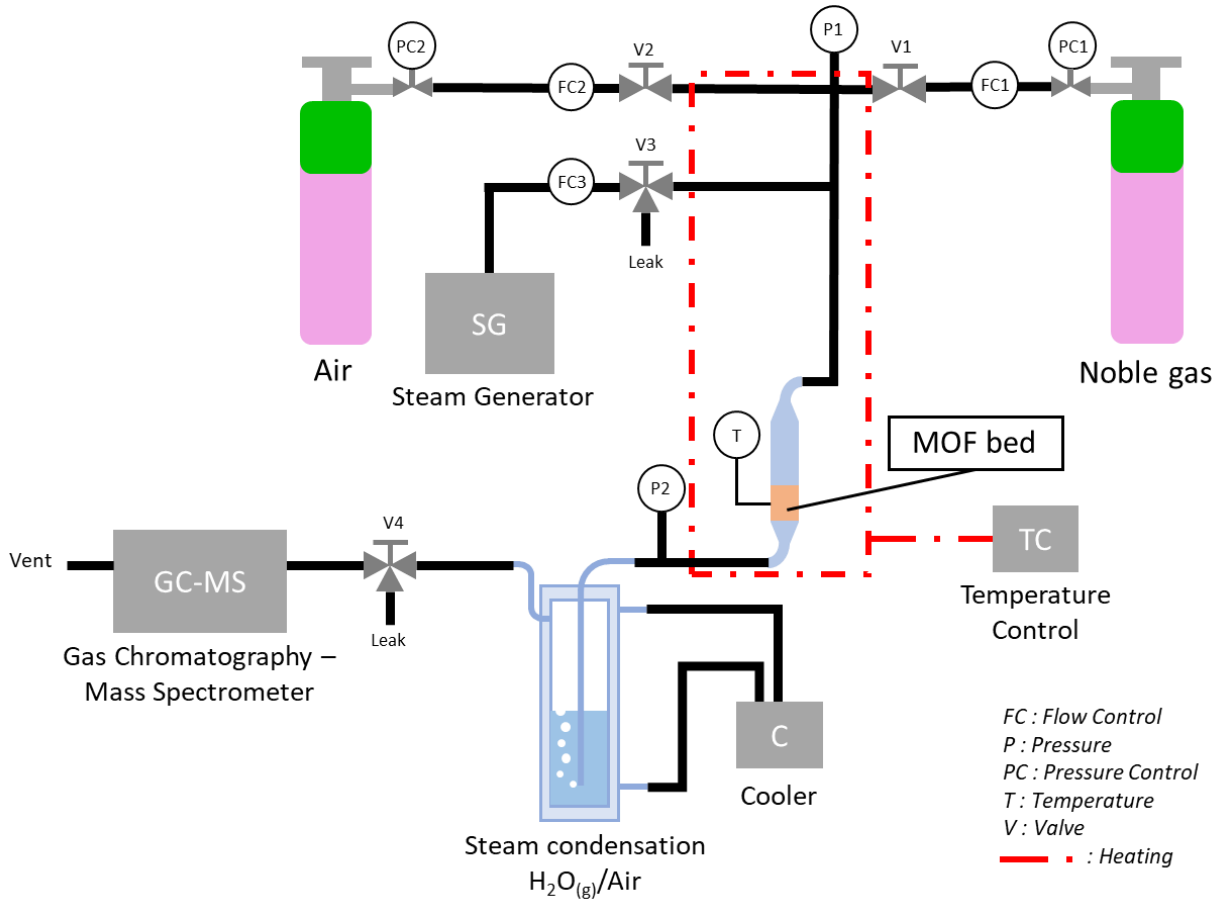

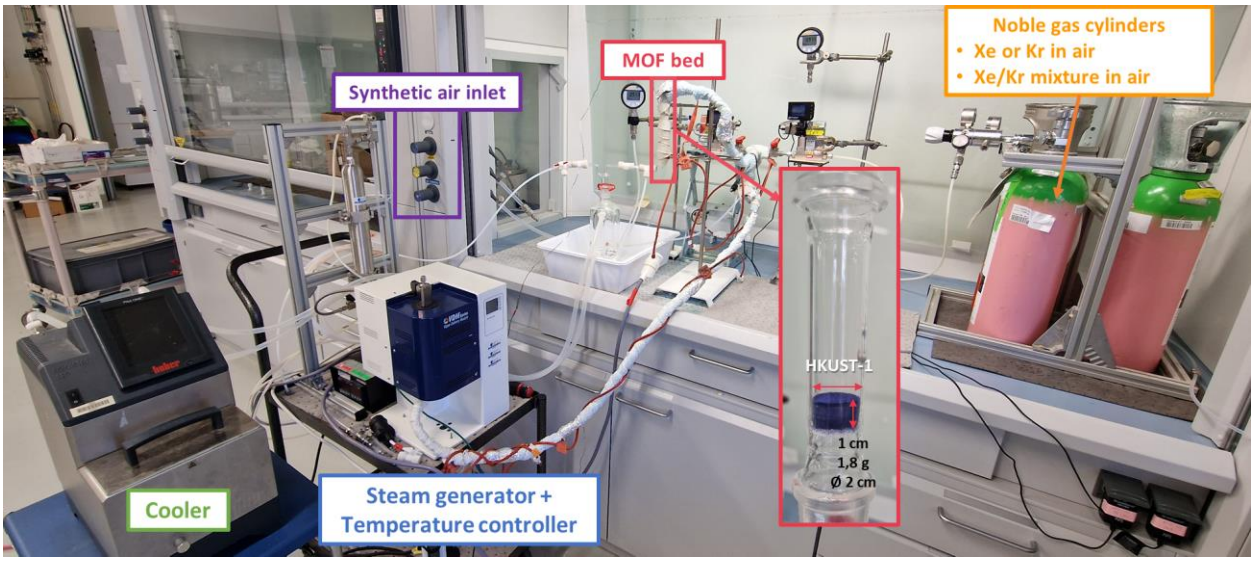

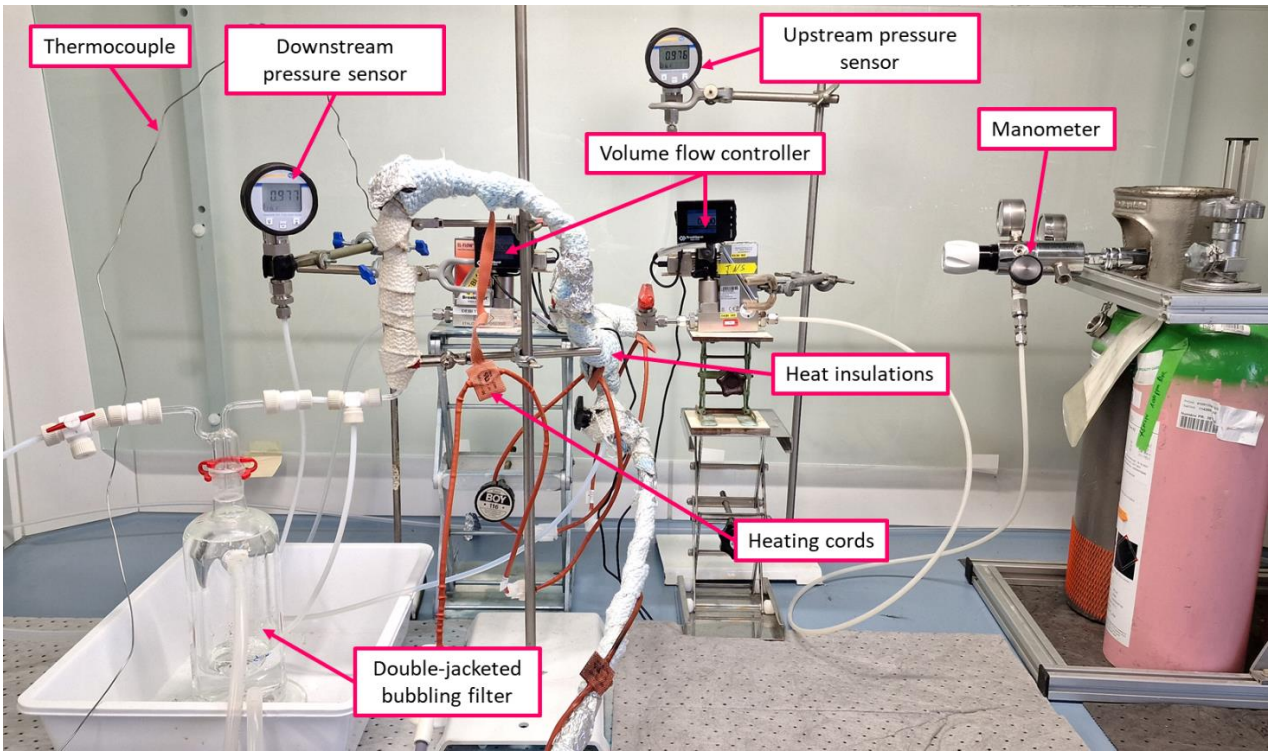

Figure S10. Experimental test bench SAFARI for dynamic adsorption of noble gases into a MOF sample.

3. Determination of Henry's constant and selectivity Xe/Kr

Static condition experiments allow selectivity to be predicted from experimentally obtained adsorption isotherms, despite injection of the noble gases separately. Xe/Kr selectivity is the ratio of the Henry's constants (k_H) [1] [2] of each gas (Equation 1). This constant is determined experimentally by applying Langmuir's linear equation to adsorption isotherms at very low pressures (Figure S11), to lie within the range of Henry's law (here Pmax < 0.05 bar with $R^2 > 0.99$), where the slope corresponds to k_H (Equation 2).

$$S_{Xe/Kr} = \frac{k_{H(Xe)}}{k_{H(Kr)}} \quad (1)$$

$$q = k_H P \; and \; k_H = Bq_m \quad (2)$$

With q the adsorbed amount ($cm^3.g^{-1}$), P the pressure (bar), k_H the Henry constant ($cm^3.g^{-1}.bar^{-1}$), B the Langmuir constant (bar^{-1}) and q_m the monolayer or saturated amount adsorbed ($cm^3.g^{-1}$).

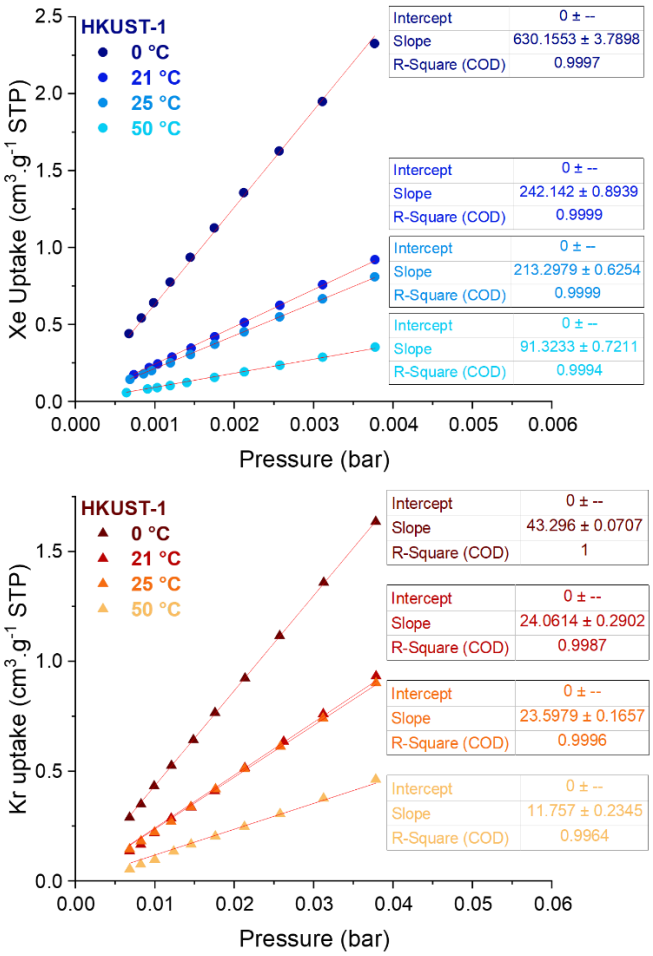

Figure S11. Determination of Henry's constant (k_H) on adsorption isotherms at low pressure (< 0.05 bar) and different temperature (0-50 °C) of Xe (top) and Kr (bottom) in HKUST-1.

4. Determination of isosteric heat of adsorption (Q_{st} and Q_{st}^0)

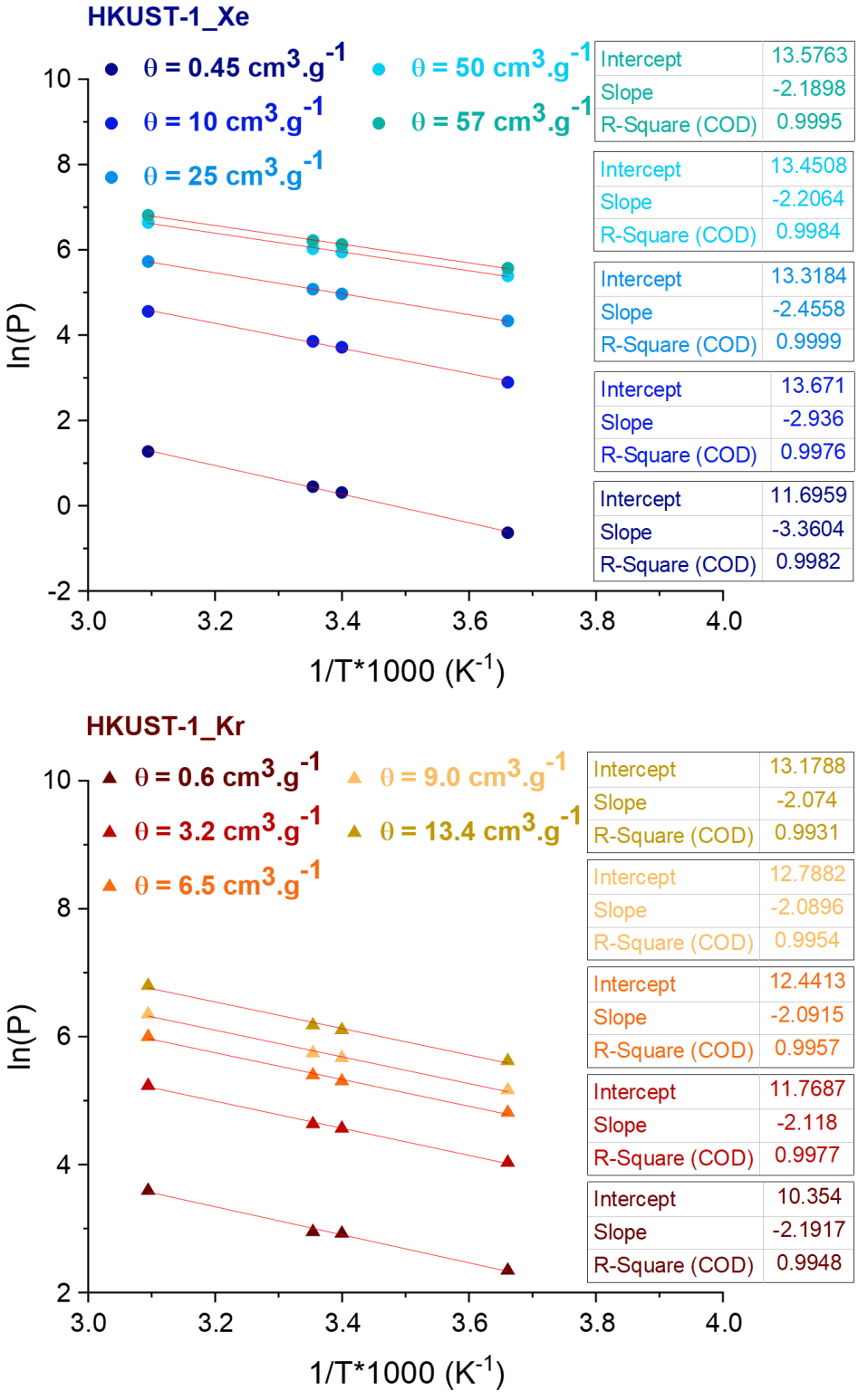

Figure S12. Determination of Q_{st} at different surface coverage (θ) for xenon (top) and krypton (bottom) in HKUST-1.

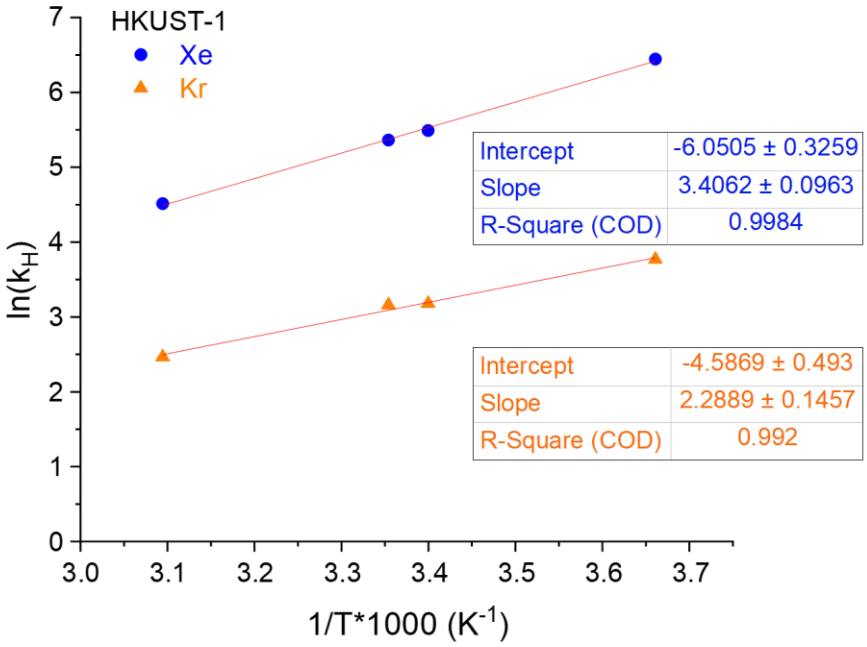

Figure S13. Determination of Q_{st}^0 at the limit of zero surface coverage (θ) for xenon (circle) and krypton (triangle) in HKUST-1.

5. Breakthrough curves of xenon in HKUST-1 material

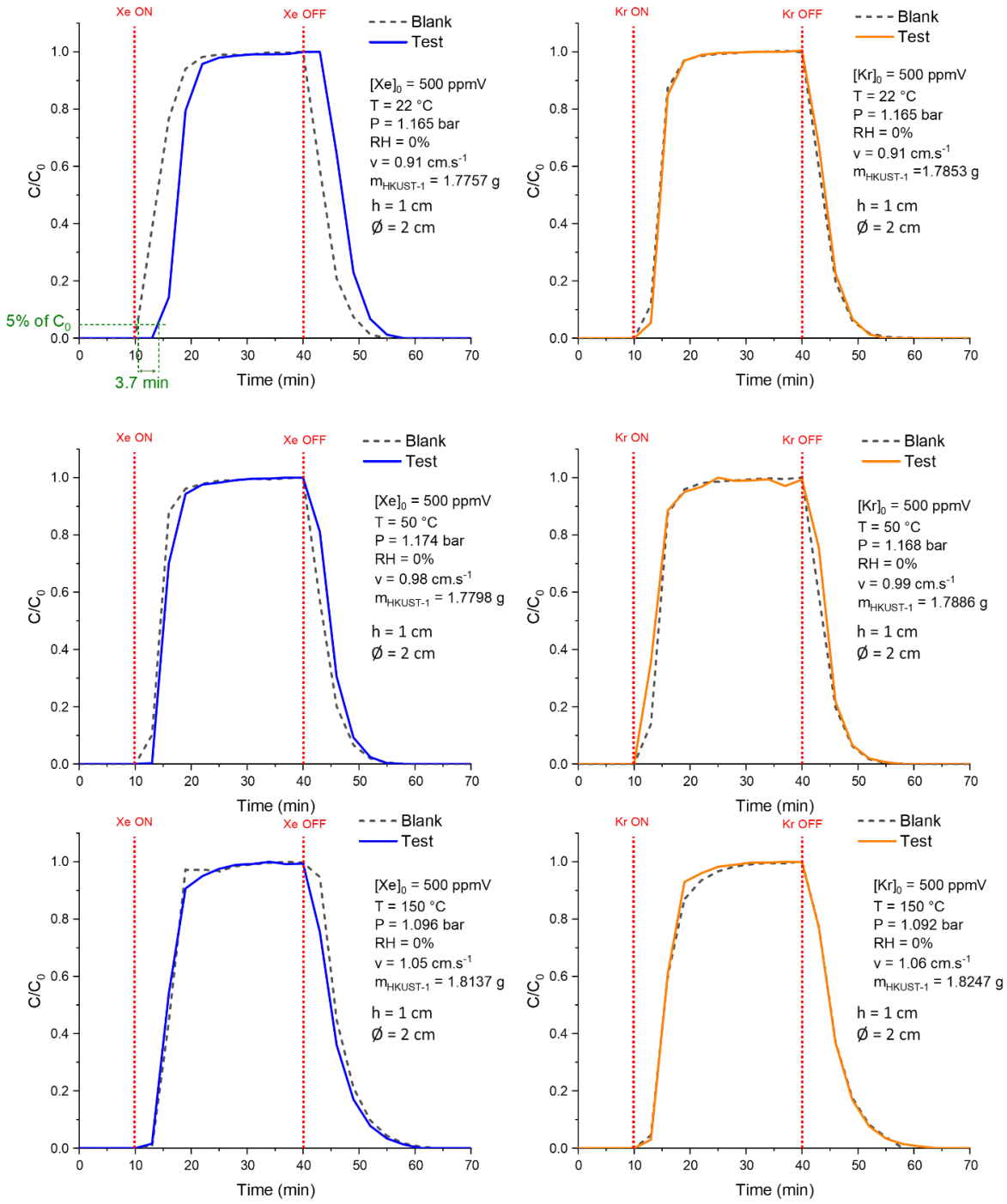

Figure S14. Xe (left) and Kr (right) breakthrough curves in HKUST-1 material on SAFARI test bench for Xe and Kr injected separately (500 ppmV in air), as function of temperature (T): 22 °C (top), 50 °C (middle) and 150 °C (bottom). The dashed curves are the test without MOF (blank) and solid curves are with (test). Pressure (P) ≈ 1 bar. Velocity (v) ≈ 1 cm.s-1. Bed height (h) = 1 cm. Column inner diameter (Ø) = 2 cm. HKUST-1 mass (m) ≈ 1.8 g. Uncertainly ± 5%.

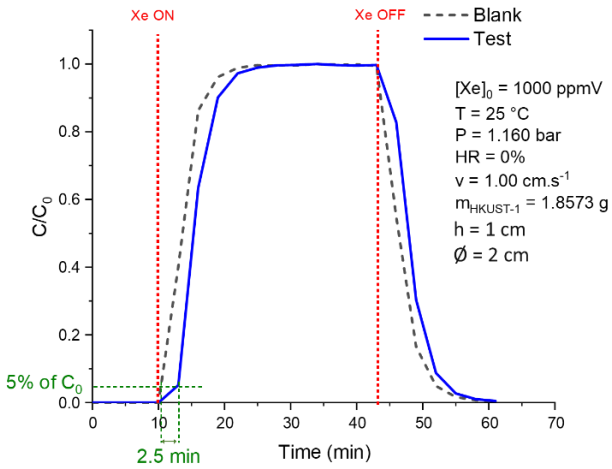

Figure S15. Xenon breakthrough curves in HKUST-1 material on SAFARI test bench for C_0 = 1000 ppmV in dry air at 25 °C. The dashed curves are the test without MOF (blank) and solid curves are with (test). Pressure (P) ≈ 1 bar. Velocity (v) ≈ 1 cm.s^{-1}. Bed height (h) = 1 cm. Column inner diameter Ø) = 2 cm. HKUST-1 mass (m) ≈ 1.8 g. Uncertainly ± 5%.

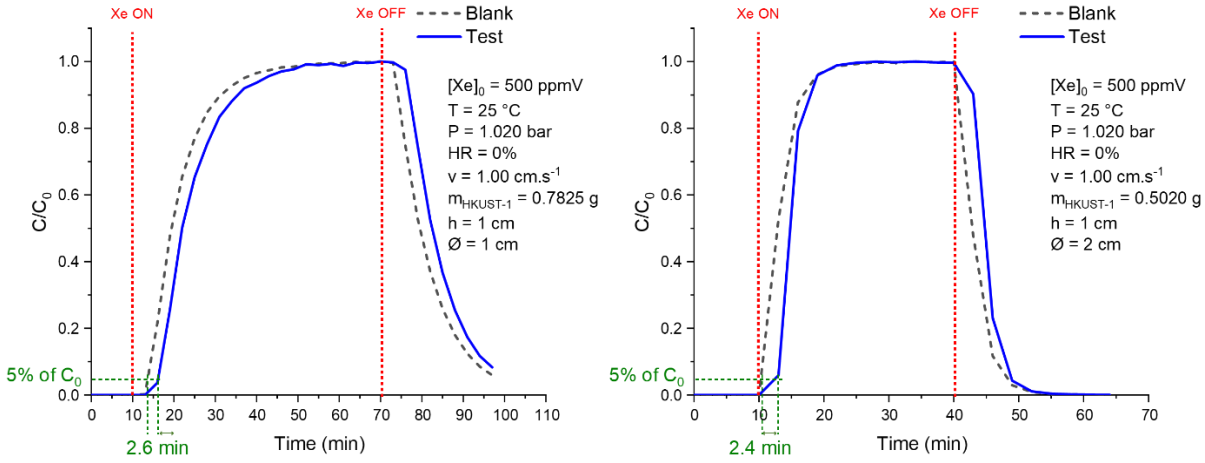

Figure S16. Xenon breakthrough curves in HKUST-1 material on SAFARI test bench for C_0 = 500 ppmV in dry air at 25 °C, and different column inner diameters (Ø): 1 cm (left) or 2 cm (right). The dashed curves are the test without MOF (blank) and solid curves are with (test). Pressure (P) ≈ 1 bar. Velocity (v) ≈ 1 cm.s^{-1}. Bed height (h) = 1 cm. HKUST-1 mass (m) ≈ 1.8 g. Uncertainly ± 5%.

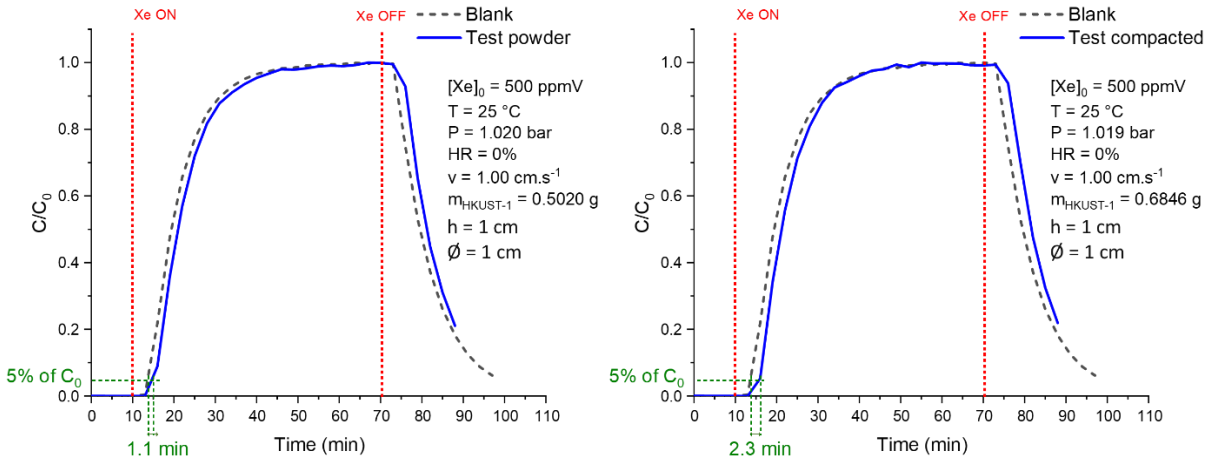

Figure S17. Xenon breakthrough curves in HKUST-1 material on SAFARI test bench for C_0 = 500 ppmV in dry air at 25 °C, for power form (left) and compacted form (right). The dashed curves are the test without MOF (blank) and solid curves are with (test). Pressure (P) ≈ 1 bar. Velocity (v) ≈ 1 cm.s^{-1}. Bed height (h) = 1 cm. Column inner diameter (Ø) = 1 cm. HKUST-1 mass (m) ≈ 0.5 or 0.7 g. Uncertainly ± 5%.

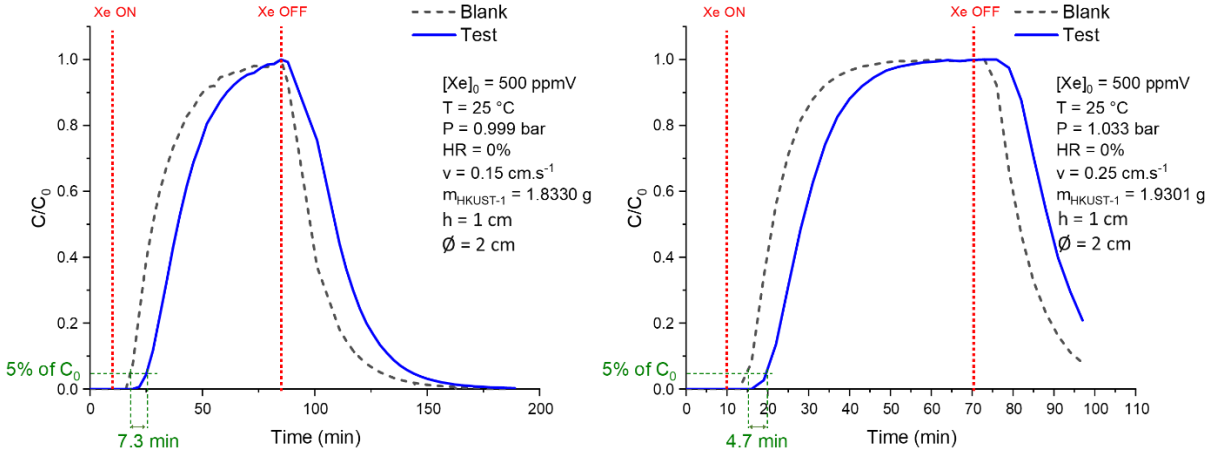

Figure S18. Xenon breakthrough curves in HKUST-1 material on SAFARI test bench for C_0 = 500 ppmV in air at 25 °C, for different velocities (v): 0.15 cm.s^{-1} (left) and 0.25 cm.s^{-1} (right). The dashed curves are the test without MOF (blank) and solid curves are with (test). Pressure (P) ≈ 1 bar. Bed height (h) = 1 cm. Column inner diameter (Ø) = 2 cm. HKUST-1 mass (m) ≈ 1.8 g. Uncertainly ± 5%.

6. SEM pictures of HKUST-1 after water exposure

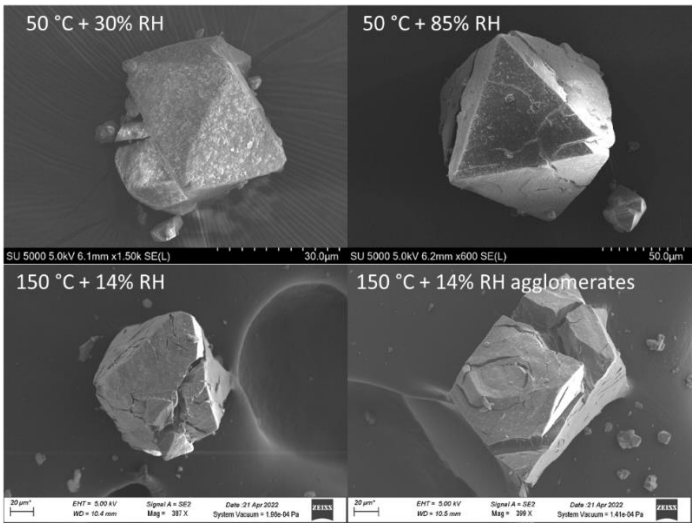

Figure S19. SEM pictures of HKUST-1 after 30-85% RH (at 50 °C) and 15% RH (at 150 °C) exposure.

REFERENCES

(1) Myers, A. L.; Prausnitz, J. M. Thermodynamics of Mixed-gas Adsorption. *AIChE journal* **1965**, *11* (1), 121–127.
(2) Yang, R. T. *Adsorbents: Fundamentals and Applications*; John Wiley & Sons, 2003.